Auto-regulatory J-domain interactions control Hsp70 recruitment to the DnaJB8 chaperone

Bryan D. Ryder[1,2], Irina Matlahov[3,5], Sofia Bali[1,2], Jaime Vaquer-Alicea[2,4], Patrick C.A. van der Wel[3,5,*], Lukasz A. Joachimiak[2,6,*]

[1] Molecular Biophysics Graduate Program, University of Texas Southwestern Medical Center, Dallas, TX 75390, United States

[2] Center for Alzheimer's and Neurodegenerative Diseases, University of Texas Southwestern Medical Center, Dallas, TX 75390, United States

[3] Department of Structural Biology, University of Pittsburgh School of Medicine, Pittsburgh, PA 15213, USA

[4] Neuroscience Graduate Program, University of Texas Southwestern Medical Center, Dallas, TX 75390, United States

[5] Zernike Institute for Advanced Materials, University of Groningen, 9747 AG Groningen, Netherlands

[6] Department of Biochemistry, University of Texas Southwestern Medical Center, Dallas, TX 75390, United States

[*] Correspondence: Lukasz.Joachimiak@utsouthwestern.edu, p.c.a.van.der.wel@rug.nl

Abstract

The Hsp40/Hsp70 chaperone families combine versatile folding capacity with high substrate specificity, which is mainly facilitated by Hsp40s. The structure and function of many Hsp40s remain poorly understood, particularly oligomeric Hsp40s that suppress protein aggregation. Here, we used a combination of biochemical and structural approaches to shed new light on the domain interactions of the Hsp40 DnaJB8, and how they regulate recruitment of partner Hsp70s. We identify an interaction between the J-Domain (JD) and C-terminal domain (CTD) of DnaJB8 that sequesters the JD surface, preventing Hsp70 interaction. We propose a new model for DnaJB8-Hsp70 regulation, whereby the JD-CTD interaction of DnaJB8 acts as a reversible autoinhibitory switch that can control the binding of Hsp70. These findings suggest that the evolutionarily conserved CTD of DnaJB8 is a regulatory element of chaperone activity in the proteostasis network.

INTRODUCTION

The cellular chaperone network needs to handle a diversity of protein substrates in numerous different (mis)folded states. This demands a combination of broad versatility and specificity in terms of substrate recognition, even though the central players Hsp70 and Hsp90 are highly conserved. This apparent contradiction is resolved by the Hsp40 (DnaJ) family of proteins, which are chaperones that recruit and regulate the activity of Hsp70 chaperones in refolding misfolded proteins[1-4]. While the human Hsp70 family is highly conserved, the Hsp40 chaperone family encodes 47 diverse members, each with specialized functions in substrate recognition and presumed coordination with Hsp70[5-7]. DnaJ proteins feature a J-domain (JD), which binds to Hsp70s through a conserved electrostatic interaction to trigger ATP hydrolysis by the Hsp70[7-10]. This initiates a conformational rearrangement in the Hsp70 substrate binding domain that helps capture the substrate for folding, refolding, or disaggregation[11]. When misfolded proteins cannot be refolded, some Hsp40s help direct them for degradation[12-13].

In humans, Hsp40s function as monomers, dimers, or oligomers. Classical Hsp40 members assemble into homo-dimers or hetero-dimers[14] through conserved C-terminal motifs and bind unfolded substrates through conserved β-barrel C-terminal domains (CTD)[15]. A subset of non-classical Hsp40s, including DnaJB2, DnaJB6b, DnaJB7 and DnaJB8 have a domain architecture that is distinct from the classical dimeric DnaJ orthologs[14-17]. These Hsp40s retain the JD, but have distinct other domains including substantial differences in their CTD structures. Of these, the DnaJB8 and DnaJB6b proteins self-assemble *in vitro* and *in vivo*[16, 18-19]. The role of their CTD remains unclear, as the literature suggests that it either drives oligomerization or mediates intramolecular contacts[16-18, 20]. The oligomers' structural and dynamic heterogeneity has greatly hindered efforts to study them, yielding for DnaJB6 limited-resolution cryoEM data[19] or requiring invasive deletion mutations to gain structural insight in soluble mutant variants[16-17].

88 Here we examine DnaJB8, which has been shown to be particularly effective at
89 preventing polyglutamine (polyQ) deposition, even more so than the homologous
90 DnaJB6b, despite 63 % sequence identity[16, 18, 20-21]. This indicates that their specific
91 modes of activity are distinct in spite of their similarities in sequence and domain
92 arrangement. Notably, unlike other chaperones that inhibit mutant huntingtin
93 aggregation[22], DnaJB8 and DnaJB6b are thought to bind directly to polyQ elements and
94 thus are active across the whole family of polyQ diseases[16, 21]. The two proteins have
95 different expression profiles, with DnaJB8 being highly expressed in testes, while
96 DnaJB6b is ubiquitous, which in part explains the deeper knowledge available for the
97 latter protein. While both DnaJB6b and DnaJB8 assemble into soluble oligomers[16, 18-19,
98 21], DnaJB8 in particular displays a higher propensity to assemble[16]. Here, we applied a
99 multidisciplinary approach to understand the architecture and dynamics of DnaJB8 in
100 cells and *in vitro*. We used crosslinking mass spectrometry (XL-MS) to identify local intra-
101 domain contacts and long-range contacts. Guided by modeling, we mutated aromatic
102 residues to create a monomeric mutant that maintains the intramolecular domain contacts
103 observed in oligomers in cells and *in vitro*. Solid-state NMR (ssNMR) probed the structural
104 and dynamic order of the solvated oligomers, to reveal dramatic domain-specific
105 differences in (dis)order and a lack of highly flexible regions. Electrostatic interactions
106 control the JD transitioning between an ordered immobilized state and a more mobilized
107 state, which we attribute to JD - CTD interactions that we reconstitute with isolated
108 domains and detect in full-length protein. Finally, we demonstrate that the JD-CTD
109 contacts regulate the recruitment of Hsp70, representing a built-in regulatory mechanism
110 that controls recruitment (and thus activation) of Hsp70.
111

112 RESULTS

113 **DnaJB8 domain interactions in a cellular context**

114 DnaJB8 encodes three domains C-terminal to the JD (Fig. 1a): a glycine and
115 phenylalanine (G/F) rich domain (Fig. 1a, blue), a serine/threonine rich (S/T) domain (Fig.
116 1a, cyan) and a C-terminal CTD (Fig. 1a, green). Prior studies have highlighted the ability

117 of DnaJB8 to assemble into oligomers but little is known about DnaJB8 domain
118 interactions in cells[16, 20]. We expressed DnaJB8 fused to a green fluorescent protein
119 (GFP) derivative mClover3 (herein, DnaJB8-Cover) in HEK293 cells (Fig. 1a). DnaJB8-
120 Clover expression leads to the formation of fluorescent juxtanuclear puncta with an
121 approximate maximum diameter of 1.0µm (Fig. 1b) in 39.2±3.1% of the cells (Fig. 1c)
122 while Clover alone expression yielded diffuse fluorescence (Fig. 1b) with little to no puncta
123 (Fig. 1c; 0.44±0.50%). The puncta observed in these cells indicate the presence of
124 ordered aggregates, while the more uniformly dispersed signal is indicative of soluble
125 oligomers and monomers. Decreasing the DnaJB8-Clover expression 3-fold as
126 determined by western blot (Supplementary Fig. 1a) and fluorescence intensity
127 (Supplementary Fig. 1b) yielded only a 2-fold decrease in the number of puncta
128 (16.2±0.08%; Fig. 1c). The frequency of puncta for Clover alone remained below 1% in
129 both experiments (Fig. 1c). Thus, even at reduced levels of expression DnaJB8 can form
130 puncta in cells.
131
132 We next sought to characterize biochemical properties of DnaJB8-Clover expressed in
133 mammalian cells. DnaJB8-Clover protein was purified using α-GFP nano-bodies[23-24]
134 (Supplementary Fig. 1c). To gain insight into the topology of DnaJB8, we employed a XL-
135 MS approach to define contacts between different domains [25-27]. Isolated DnaJB8-Clover
136 was reacted with adipic acid dihydrazide (ADH) and 4-(4,6-dimethoxy-1,3,5-triazin-2-yl)-
137 4-methyl-morpholinium chloride (DMTMM). ADH covalently links carboxylate-carboxylate
138 contacts via a 6-carbon bridge, while DMTMM forms a direct covalent bond between
139 lysine-carboxylate groups through dehydration[26]. Crosslinking treatment of the purified
140 soluble DnaJB8-Clover species revealed predominantly monomers and dimers in the
141 cells, with a trace of larger oligomers (Supplementary Fig. 1d). We identified 21 crosslinks
142 that parsed into 3 regions: JD-JD, CTD-CTD and JD-CTD (Fig. 1d, Supplementary Data
143 1). The three local JD contacts (Fig. 1d; red box) are consistent with its experimental
144 structure (Supplementary Fig. 1e). Local CTD contacts (Fig. 1d, green box) were also
145 accompanied by inter-domain JD-CTD contacts that localize to helices 2 and 3 of JD (Fig.
146 1d, grey box). Additionally, we identified a contact between the JD and a putative helix 5

147 (Fig. 1d, H5) of the G/F domain, as also recently identified in DnaJB6b[17]. Thus, soluble
148 DnaJB8-Clover species isolated from mammalian cells reveal an array of inter-domain
149 interactions, including contacts between the charge complementary JD and CTD.
150

151 **DnaJB8 domain contacts are preserved *in vitro***

152 For a more detailed understanding of DnaJB8 domain architecture *in vitro*, we produced
153 recombinant DnaJB8 as described previously[16]. We first used Dynamic Light Scattering
154 (DLS) to monitor the hydrodynamic radius (R_h) of DnaJB8 species over time. The
155 scattering data reveals *bona fide* DnaJB8 sizes which begin as a small 4.28±0.82nm
156 species with a small (<%1 by mass) contribution of larger species (>10nm) but over time
157 these small species shift to 5.35±0.22 nm at 10 hours and to 5.77±0.43 nm after 20 hours
158 (Fig. 1e and Supplementary Fig. 1f). Over the time course, a fraction of the soluble small
159 species converted into larger oligomers >10nm (30.6% by mass) with an average R_h of
160 90nm (Fig. 1e and Supplementary Fig. 1f). These findings are consistent with prior studies
161 on DnaJB6b and DnaJB8 showing that they have the capacity to assemble into
162 polydisperse soluble oligomers *in vitro*[16, 18-19, 21, 28].
163

164 Next, we aimed to better understand the topology of DnaJB8 *in vitro* using XL-MS,
165 employing two parallel chemistries; disuccinimidyl suberate (DSS) and ADH/DMTMM on
166 samples after a brief 30 mins of incubation. Consistent with the DLS data at early time
167 points, we observe by SDS-PAGE a ladder of bands indicating the formation of covalent
168 intermolecular contacts dominated by a dimer (Supplementary Fig. 1g). XL-MS analysis
169 of these samples showed only 3 crosslinks in the DSS condition (Fig. 1f, Supplementary
170 Data 1). In contrast, the ADH/DMTMM analysis yielded 24 crosslinks (Fig. 1f,
171 Supplementary Data 1). Importantly, this XL-MS pattern persisted across the DLS time
172 course (Supplementary Fig. 1h and Supplementary Data 1) and closely matches the pairs
173 observed in the assemblies recovered from the mammalian cells including crosslinks from
174 both JD and CTD to H5 (Fig. 1d, H5). The JD crosslinks are consistent with the structure
175 of the domain (Supplementary Fig. 1i)[26].
176

177 The CTD yielded 8 crosslinks (Fig. 1f). Amongst these, the locally-linked regions spanning
178 E208-E211 and K223-K227 are central to the CTD and repeatedly react to peripheral
179 sites. The third cluster of contacts linked the distal JD and CTD through 4 crosslinks (Fig.
180 1f; JD:CTD). The interdomain CTD crosslink sites are exclusively mediated through acidic
181 amino acids; D212, E209 and E211. Interestingly, the crosslinked amino acids on the JD
182 are all lysines that localize to basic surfaces along helix 1 and 2 (Supplementary Fig. 1j)
183 and overlap the basic Hsp70 binding surface[10]. These XL-MS data identify an intricate
184 network of electrostatic inter-domain interactions in both monomeric and oligomeric
185 DnaJB8.
186
187 To further test the apparent role of electrostatically driven interactions, we used a higher
188 ionic strength buffer in an analogous series of experiments. Using DLS we observed a
189 defined species with a 7.75±0.7nm size in 285mM NaCl (Fig. 1g, Supplementary Data 2),
190 which are more expanded compared to species in 150mM NaCl (Fig. 1e, Supplementary
191 Data 2). XL-MS analysis recapitulates the short-range contacts within the JD and CTD
192 domains but the JD:CTD contacts were notably absent (Fig. 1h). To control for reactivity
193 in each condition we compared the frequency of ADH-driven singly reacted modifications,
194 called monolinks. These data show nearly identical numbers of modifications suggesting
195 that the reactivity between these two conditions is nearly identical (Supplementary Fig.
196 1k). Thus, the disruption of electrostatically driven interactions is accompanied by
197 changes in the domain architecture.
198
199 **JD:CTD interaction is mediated by electrostatic contacts**
200 To understand how the JD and CTD domains could be interacting, we used Rosetta
201 modeling guided by XL-MS restraints. We built a starting model by combining the
202 experimental structure of the JD (PDBID: 2DMX) with an *ab initio*-derived model for CTD
203 and the middle domains fully extended. The starting model was then collapsed by
204 applying the JD-CTD crosslinks as restraints (Fig. 2a and Supplementary Fig. 2a-b). The
205 fully expanded monomer collapsed from a predicted R_h of 9.27 nm (R_g, 6.65 nm) to 4.02

206 nm (R_g, 2.45 nm) (Fig. 2a). Comparing these values to our DLS radii in 150mM NaCl
207 suggests that the dominant species are likely monomers and dimers. The DLS
208 measurements in 285mM NaCl are consistent with the initial expanded model with the
209 JD:CTD contacts disengaged. Thus, our data support that DnaJB8 exists in solution as
210 small soluble species (4 to 6 nm), dominated by monomer/dimer but with capacity to form
211 larger oligomers over time, both *in vitro* and *in vivo*.
212
213 Guided by the constraints, the final model "docks" the JD onto the CTD placing a putative
214 acidic surface on the CTD in contact with the basic surface on the JD (Fig. 2a and
215 Supplementary Fig. 2b) and additionally bringing H5 in proximity to both the JD and CTD
216 as similarly observed for DnaJB6b (Supplementary Fig. 2c) [17]. The CTD has proximal
217 basic surfaces that flank its acidic surface, generating a characteristic alternating charge
218 pattern that is inverted on the JD (Fig. 2c). Mapping sequence conservation onto the
219 Rosetta-generated model, we find that these JD:CTD contacts are largely conserved
220 (Supplementary Fig. 2d). In a co-evolution analysis using the Gremlin algorithm[29-31] we
221 identified amino acid positions that covary. Not only did we observe many amino acid
222 pairs that covary between the JD and CTD as well as H5, but our XL-MS pairs overlap
223 with these covarying positions (Fig. 2d). The similarity between the predicted covarying
224 contacts, conservation, and the XL-MS experimental contacts strengthens our DnaJB8
225 JD-CTD model, and suggests that XL-MS can detect functionally important interaction
226 sites.
227
228 **JD:CTD contacts are present in monomeric DnaJB8**
229 In our "collapsed" monomer structural model the 17 phenylalanine residues in the G/F
230 and S/T domains were predicted to be in part solvent exposed (Fig. 2a, spheres). We
231 hypothesized that these aromatic residues may play a role in DnaJB8 assembly and
232 engineered a mutant, in which all G/F- and S/T-region phenylalanine residues were
233 mutated to serine residues (Fig. 2e, herein DnaJB8$_{F\rightarrow S}$). Using our DLS and XL-MS
234 pipeline, we evaluated assembly of DnaJB8$_{F\rightarrow S}$. By DLS, the DnaJB8$_{F\rightarrow S}$ mutant

235 remained stable as a 3.53±0.05 nm species over 21 hours (Fig. 2f, Supplementary Data
236 2). SDS-PAGE of crosslinked DnaJB8$_{F\rightarrow S}$ also showed no intermolecular crosslinks.
237 (Supplementary Fig. 2e). Size Exclusion Chromatography Multi-Angle Light Scattering
238 (SEC-MALS) analysis on DnaJB8$_{F\rightarrow S}$ revealed it to be a monomer with a molecular weight
239 of 24,530±30 g/mol (Fig. 2g). These data support that phenylalanine residues in the G/F
240 and S/T domains play a role in higher order assembly. Next, we used XL-MS to test
241 whether this DnaJB8$_{F\rightarrow S}$ monomer maintained the intramolecular JD and CTD contacts
242 observed in WT DnaJB8 (Fig. 2h). Analysis of the crosslinked DnaJB8$_{F\rightarrow S}$, revealed
243 identical local crosslinks within JD and CTD and also detected 3 crosslinks between the
244 JD and CTD. Interestingly, in DnaJB8$_{F\rightarrow S,}$ the H5 crosslinks to JD were absent, consistent
245 with requirement of a phenylalanine in H5 for binding to the JD (Fig. 2h, H5). The
246 presence of the JD-CTD crosslinks in a monomeric mutant marks them to represent
247 *intra*molecular JD:CTD interactions.
248
249 We can now use the experimental DLS radii with our structural models to more accurately
250 infer the dimensions of the small soluble DnaJB8 species (Fig. 2i). At the start of the WT
251 DnaJB8 DLS time course, we observed an initial population of polydisperse particles with
252 an average radius of 4.28±0.82nm (Fig. 1e). The DnaJB8$_{F\rightarrow S}$ mutant showed a radius of
253 3.53±0.05nm with a very narrow monodisperse distribution, further supporting our model
254 of a monomer "collapsed" by JD:CTD interactions. Based on a model proposed by Marsh
255 and Forman-Kay[32], we also estimate that a monomeric 232-residue DnaJB8 protein
256 should have a size of 3.98 nm. These data support our analysis that WT DnaJB8 at first
257 adopts primarily a monomer/dimer distribution that has the capacity to then assemble into
258 large oligomers. In contrast, the larger DLS R_h values measured for DnaJB8 in 285mM
259 NaCl (Fig. 1g), are a result of the loss of the JD:CTD contacts yielding a small oligomer
260 mediated by aromatic contacts.
261
262 **ssNMR on DnaJB8 oligomers reveals regions of disorder and order**
263 For additional insight into their molecular structure and dynamics, magic-angle-spinning

264 (MAS) ssNMR was performed on the hydrated oligomers of U-^{13}C,^{15}N-labeled DnaJB8.
265 MAS ssNMR of hydrated protein assemblies allows for the site- and domain-specific
266 detection of mobility and (secondary) structure, even in presence of disorder and
267 heterogeneity. 1D and 2D ssNMR spectra of the DnaJB8 oligomers feature many broad
268 peaks, with linewidths up to 0.38 kHz, consistent with an oligomeric assembly displaying
269 structural disorder (Fig. 3a; Supplementary Fig. 3a-d). However, strikingly, distinct
270 subsets of narrow peaks are also detected, with linewidths of 0.1 to 0.2 kHz (Fig. 3c-d
271 left). These ssNMR experiments employ the cross-polarization (CP) technique, in which
272 observable residues must be rigid or immobilized[33]. In INEPT-based ssNMR, which is
273 selective for highly dynamic segments, the oligomers show little signal[33-36] (more below).
274 Then, the observed narrow signals in CP spectra must originate from an immobilized,
275 well-ordered subset of DnaJB8 residues. These narrow signals are from amino acid
276 types[37] in the JD while the broad peaks are dominated by signals from residues common
277 in other domains (Supplementary Table 1). The former also reflect mostly α-helical
278 structure, while the latter are mostly random coil and β-sheet [38]. With known chemical
279 shifts of the DnaJB8 JD in solution, we prepared a synthetic 2D spectrum (Supplementary
280 Fig. 3b red) that has a striking correspondence to the narrow ssNMR peaks
281 (Supplementary Fig. 3b black), such that we tentatively assign those to residues in helix
282 2 and helix 3. The 2D ^{15}N-^{13}Cα (NCA) ssNMR spectrum showed a similar alignment
283 between narrow peaks and JD signals in solution (Supplementary Fig. 3d). These CP-
284 based 2D spectra also feature strong peaks from immobilized charged side chains (Lys,
285 Arg, Asp, Glu; Supplementary Figure 3e-f), which is consistent with their involvement in
286 salt-bridge interactions predicted by the XL-MS analysis above.
287 In absence of experimental solution NMR data for other domains, we predicted
288 estimated spectra based on our structural models (Fig. 3c-d green; Supplementary Fig.
289 3c)[39]. These peak patterns qualitatively resemble the broad signals in our 2D ssNMR
290 data. A particular strength of MAS ssNMR of hydrated proteins is the ability to gauge local
291 and global dynamics. Single pulse excitation (SPE) and refocused INEPT spectra, which
292 enhance the more dynamic parts of samples[35-36] show surprisingly little evidence of

293 flexible residues (Fig. 3e top red). Indeed, the main INEPT signal (~42 ppm) is just from
294 solvent-exposed Lys side chains and lacks evidence of flexible protein regions (even from
295 the S/T or G/F regions). Given that the 1D CP and SPE spectra (Fig. 3e top) look similar,
296 with higher signal intensities in the former, the different domains of the protein actually
297 must have a similar degree of mobility and all be mostly immobilized, without flexible
298 regions. Combined, the ssNMR data reveal oligomers that are heterogeneous in structure
299 but lack extended flexible domains. In other words, the central G/F and ST domains are
300 heterogenous, but also immobilized within the oligomers, consistent with the
301 abovementioned role of their Phe residues in driving oligomer assembly. Uniquely
302 ordered are parts of the JD (residues in helices 2 and 3; Supplementary Fig. 3g,h), which
303 show up as well-folded and immobilized.
304
305 **Interaction sites from ssNMR**
306 MAS ssNMR studies of DnaJB8 oligomers in PBS buffer with 285mM NaCl (analogous
307 to the studies above) are shown in Fig. 3b. The 2D spectrum reproduces the broad signals
308 of the immobilized oligomers, but the narrow JD peaks are now strikingly absent.
309 Comparing CP and SPE ssNMR spectra (Fig. 3e bottom), there is an increase in overall
310 mobility. Notably, no new "flexible" ssNMR signals were identified by INEPT ssNMR. We
311 attribute the loss of JD signals in CP-based spectra to increased mobility due to disruption
312 of long-range electrostatic interactions, while the lack of INEPT peaks tells us the JD is
313 still folded and partly immobilized by covalent attachment to the overall assembly. In other
314 words, the JD is invisible due to intermediate timescale dynamics[33, 40]. Since the broad
315 signals from the other domains are preserved, it appears that the core architecture of the
316 oligomers persists, consistent with aromatic and hydrophobic interactions.
317
318 **Isolated JD and CTD are folded and monomeric**
319 To further characterize the JD and CTD interaction, we produced isolated JD (herein JD_{1-}
320 $_{77}$) and CTD (herein $CTD_{170-232}$) (Fig. 4a). SEC analysis of JD_{1-77} and $CTD_{170-232}$ revealed
321 monodispersed peaks (Fig. 4b). SEC-MALS determined each domain to be monomeric

322 with a molecular weight of 10,220±220 g/mol and 8,376±14 g/mol for JD_{1-77} and CTD_{170-}
323 $_{232}$, respectively (Supplementary Fig. 4a-b). Also, by DLS we measured the JD_{1-77} R_h to
324 be 2.31±0.13 nm and the $CTD_{170-232}$ to be 1.71±0.02 nm, with both stable over 15 hours
325 (Supplementary Fig. 4c, Supplementary Data 2). We again employed XL-MS to probe the
326 individual domains and compare them to full-length protein. On an SDS-PAGE gel, the
327 crosslinked JD_{1-77} and $CTD_{170-232}$ remained monomeric following crosslinking (Fig. 4c).
328 XL-MS analysis yielded 4 crosslinks for JD_{1-77} and 6 crosslinks for $CTD_{170-232}$ (Fig. 4d,
329 Supplementary Data 1). The identified crosslinks revealed good agreement between the
330 local domain crosslinks observed in the full-length DnaJB8 and the isolated domains (Fig.
331 4d, Supplementary Fig. 4d).
332 We built an ensemble of models for the $CTD_{170-232}$ using *ab initio* ROSETTA[40]. The
333 calculated R_h for the structural ensemble was consistent with the DLS measurement of
334 1.7 nm (Supplementary Fig. 4g). The models formed a low contact order 5-stranded β-
335 sheet topology and the R_h variation can be attributed to the more flexible termini
336 (Supplementary Fig. 4g, inset). Circular dichroism (CD) on the CTD sample yields spectra
337 consistent with a predominantly β-sheet content, as predicted by our model
338 (Supplementary Fig. 4e-f). We mapped the 14 CTD-derived crosslinks from across
339 experiments onto the monomeric ensemble, finding that a majority of structures explain
340 10-11 crosslinks but only a single model explains 13 of 14 (Fig. 4e). These crosslink pairs
341 map onto each face of the β-sheet and the distances are compatible with the geometry
342 of the crosslinking chemistry. The crosslinks that fall outside of the distance cutoff localize
343 to the more dynamic C-terminus of CTD (Fig. 4e and Supplementary Fig. 4g, inset) at
344 positions K227 and K223. The CTD topology is defined by four β-turns stabilized by
345 conserved asparagine/aspartate-glycine sequences (N/DG) and overlays well with the
346 DnaJB6b CTD (Fig. 4f)[17]. Thus, our data support that both the JD_{1-77} and $CTD_{170-232}$
347 domains are folded, monomeric, and do not have intrinsic assembly properties.
348
349 **Basic surface on JD drives interaction with CTD**

350 In our experiments on the full-length DnaJB8 oligomers we observed that the JD and CTD
351 interact through complementary electrostatic surfaces. We further probed this interaction
352 by mixing the individual JD_{1-77} and $CTD_{170-232}$ domains *in vitro* (Fig. 5a). We incubated
353 Flourescein(FITC)-labelled JD_{1-77} with a series of $CTD_{170-232}$ concentrations and
354 measured binding affinity using a fluorescence polarization (FP) assay. The resulting
355 binding curve revealed that the JD_{1-77} binds to the $CTD_{170-232}$ with 0.542±0.071 μM affinity
356 (Fig. 5a; bottom). Parallel experiments using Microscale Thermophoresis revealed a K_d
357 of 5.36±1.15 μM (Supplementary Fig. 5a) suggesting that the affinity is in the low
358 micromolar range. JD_{1-77} and $CTD_{170-232}$ domains were mixed together to form the
359 complex and analyzed using XL-MS. We identified 6 local crosslink pairs consistent with
360 pairs observed in full-length DnaJB8 and the isolated JD_{1-77} and $CTD_{170-232}$ samples (Fig.
361 5b). Importantly, we also reconstitute 4 intermolecular contacts between the JD_{1-77} and
362 $CTD_{170-232}$ observed in full length DnaJB8 experiments. However, an increased variance
363 in the crosslink profile may indicate that the missing proximal sequences help define the
364 proper architecture of the full-length DnaJB8 oligomers. Solution NMR-based chemical
365 shift perturbation (CSP) mapping was used to identify the JD_{1-77} surface that interacts
366 with the $CTD_{170-232}$ (Fig. 5c, Supplementary Fig. 5b-c). Titration of increasing amounts of
367 unlabeled $CTD_{170-232}$ into ^{15}N-labeled JD_{1-77} produced fast exchanging concentration-
368 dependent CSPs in a specific subset of peaks (Fig. 5d-e); 33 peaks were strongly
369 perturbed (>0.2 p.p.m.) and another 40 peaks were perturbed weakly (>0.1 p.p.m.).
370 Among the strongly perturbed peaks, 27 residues have solvent accessible side chains of
371 which fifteen are charged, with a notable overlap with the basic face in helix 2 that is
372 implicated in Hsp70 binding (Fig. 5f-h). Other residues that show strong perturbations are
373 basic and acidic residues that wrap around the exterior of the JD loop and helix 3, and
374 residues on the charged face of helix 4. While a few other hydrophobic residues also
375 show strong perturbations, all are in close proximity to charged residues along each helix.
376 Given the small size of the JD_{1-77}, it is likely that residues in the core behind the basic
377 surface involved in the interaction experience changes in chemical shift.
378

379 **JD-CTD interaction competes with Hsp70 binding**

380 The recent X-ray structure of the DnaK:DnaJ complex revealed a conserved charge-
381 based interaction between the basic surfaces on the JD of DnaJ and an acidic surface on
382 DnaK[10]. Using this complex as a template, we modeled the binding interface of the human
383 Hsp70 (HspA1A)[41] and the JD of DnaJB8[42] (Fig. 6a-c). The basic surface on the DnaJB8
384 JD (Fig. 6b) contacts the conserved acidic surface on HspA1A (Fig. 6c, Supplementary
385 Fig. 6a-b). Thus, conserved electrostatic contacts are likely to play a key role in the
386 interaction between Hsp70 and Hsp40.

387

388 The conserved HspA1A-JD electrostatic contacts (Fig. 6b-c) that overlap with the JD-CTD
389 contact sites lead us to hypothesize that the observed JD-CTD interactions could interfere
390 with Hsp70 binding. To test this hypothesis, we employed a competition experiment
391 leveraging our FP binding assay to discriminate the JD-CTD and JD-HspA1A complexes
392 (Fig. 6d). We determine a 0.257±0.029μM affinity for the JD:HspA1A interaction,
393 consistent with values in the literature[43] and similar to the JD:CTD interaction (Fig. 6e,
394 black and green, respectively). Due to the size difference between HspA1A (70 kDa) and
395 the CTD (8.7 kDa) their respective complexes with tagged JD plateau at different
396 polarization values (Supplementary Fig. 6c, black and green, respectively). Leveraging
397 this difference, we designed a binding experiment to measure the competition of HspA1A
398 and CTD binding to the JD. FITC-labeled JD was preincubated with 3 μM CTD, followed
399 by a titration with HspA1A. The pre-titration FP signal was consistent with formation of
400 the JD-CTD complex, which persisted until HspA1A concentrations of 3.125uM when the
401 signal shifted to that of a JD-HspA1A complex (Supplementary Fig. 6c, purple).
402 Normalization of the data reveals a ~25-fold decrease in the apparent binding constant
403 between JD:HspA1A when preincubated with CTD (Fig. 6e). To further test the inhibitory
404 role of CTD on recruitment of Hsp70, we used XL-MS to measure the frequency of
405 HspA1A and JD contacts across a set of complexes formed between HspA1A and WT
406 DnaJB8, $JD_{1\text{-}77}$, $DnaJB8_{F\rightarrow S}$ and DnaJB8ΔCTD missing the CTD (Fig. 6f). Across three
407 experiments, we detected no crosslinks between the Hsp70 and the JD in WT DnaJB8

408 and only 2 in DnaJB8$_{F\rightarrow S}$ (Fig. 6g, Supplementary Data 1). In contrast, in the HspA1A:JD$_{1-}$
409 $_{77}$ and HspA1A:DnaJB8ΔCTD complexes, we identified 47 and 14 total crosslinks
410 between the JD and HspA1A, respectively (Fig. 6g). All identified pairs are consistent with
411 the structural model (Fig. 6h and Supplementary Fig. 6d). These data support that the
412 robust JD:CTD engagement seen in WT DnaJB8 and even the monomeric DnaJB8$_{F\rightarrow S}$
413 (Supplementary Fig. 6e) prevents HspA1A interaction with the JD domain and deletion of
414 the CTD releases the inhibitory effect (Fig. 6g). Thus, the DnaJB8 JD uses a basic surface
415 to bind an internally encoded CTD via an acidic surface that directly inhibits HspA1A
416 binding.
417

418 DISCUSSION

419

420 **Modeling the shape of DnaJB8**

421 DnaJB8, like DnaJB6b, has the capacity to assemble into soluble oligomers. We used a
422 combination of protein engineering, solution scattering data and modeling to understand
423 the shapes of DnaJB8 in solution. Using our XL-MS data, we collapsed a DnaJB8
424 structural model around the JD:CTD interaction and thus obtained a structural model that
425 fit the average R_h of the monomer measured by DLS. Based on the fold of this monomeric
426 model, we hypothesized that aromatic amino acids in the central G/F and S/T domains
427 would be exposed and thus could mediate self-assembly into oligomers. Indeed,
428 mutagenesis of aromatic residues yielded a stable monomeric variant of DnaJB8 in
429 agreement with our collapsed structural model with engaged JD:CTD contacts. This is
430 further supported by good agreement between the R_h of our collapsed structural model,
431 DLS data, and values derived from the Marsh and Forman-Kay model[32]. An intriguing
432 question relates to whether our models may also be applicable to DnaJB6b. At this time
433 a direct comparison is difficult given the known structural and functional differences of the
434 proteins and the lack of analogous experimental data, especially on the larger oligomers
435 of DnaJB6b. Our collective data highlights the power of our multipronged approach to

436 derive the base unit of a DnaJB8 monomer, which employs exposure of aromatic residues
437 to mediate assembly through nonpolar surfaces into larger oligomers.
438
439 **Functional role of the CTD in DnaJB8**
440 We combined XL-MS and NMR in the solid and solution states to probe DnaJB8 inter-
441 domain interactions. One of the most striking features was a newly identified interaction
442 between the distal JD and CTD driven by electrostatics. This interaction was perturbed
443 by the addition of salt, but maintained following mutagenesis of aromatic amino acids in
444 the central domains. Since analysis of the isolated JD and CTD showed a reduced mutual
445 association, there nonetheless is a distinct role for the intervening domains in the JD-CTD
446 interaction. Our combined data show that the DnaJB8 S/T and G/F domains are not
447 behaving as "flexible linkers"[17] and that their aromatic residues are central in the homo-
448 oligomerization process. On their own, both JD and CTD are surprisingly resistant to self-
449 assembly. These findings are distinct from published reports on DnaJB6b, where the CTD
450 appears to drive oligomerization, which may relate to sequence divergence in the six C-
451 terminal CTD residues between DnaJB8 and DnaJB6b[17-18]. Nonetheless, our modeled
452 CTD structure, featuring a pleated β-sheet topology absent of a hydrophobic core, is
453 identical to its recently reported DnaJB6b counterpart[17]. Interestingly, outside of inter-
454 strand hydrogen bonding and polar side-chain contacts, it is not clear what forces stabilize
455 this domain. This may explain the CTD heterogeneity (unlike the JD) seen by ssNMR.
456 The CTD topology resembles the charged β-sheet surface on Hsp70 that is known to
457 interact with the JD[10]. While our reconstitution of the JD:CTD interaction using isolated
458 domains indicates that the CTD alone can bind the JD, we cannot exclude that helix 5
459 can contribute to this interaction to regulate Hsp70 function. It is worth noting that lysine
460 residues in the DnaJB8 and DnaJB6b CTD can be acetylated and deacetylated (via
461 Histone Deacetylases (HDACs)) to modify these proteins' self-assembly and function,
462 which may involve changes in the Lys-mediated JD interactions[16, 20]. The CTD
463 architecture is conserved in a broader subset of B family member Hsp40s[18]. We speculate
464 that the CTD in these DnaJB family members similarly serves a regulatory role in which

465 post-translational modifications could alter the affinity for the JD, and thus indirectly alters
466 oligomerization or Hsp70 recruitment.
467
468 **Implications for Hsp70 recruitment and substrate binding.**
469 Aside from suppressing protein aggregation on its own[16, 18, 20], DnaJB8 also recruits
470 Hsp70 for processing of bound substrates. Our current findings hint at an intriguing
471 possibility that auto-inhibitory interactions of the Hsp70-binding JDs within the DnaJB8
472 oligomer could be involved in substrate-binding-coupled Hsp70 recruitment. In the non-
473 stressed native state, DnaJB8 forms soluble oligomers in which the JD is engaged in
474 electrostatic interactions and thus not available for Hsp70 binding as supported by our
475 experiments (Fig. 6g; Fig. 7a). We hypothesize that substrate binding could allosterically
476 disrupt the JD-CTD interaction, exposing the Hsp70-binding HPD motif of the JD (Fig.
477 7b). This would enable the recruitment of Hsp70 to the loaded DnaJB8 protein. Aromatic-
478 driven oligomeric assembly of DnaJB8 may be related to the formation of liquid-liquid
479 phase separated assemblies in other proteins containing similar arrangements of
480 phenylalanine residues[44]. We propose that the more hydrophobic elements of the G/F
481 and S/T domains form the oligomer core, with the CTD and JD remaining relatively
482 surface exposed. Thus, it may be possible to recruit Hsp70 to different DnaJB8 species.
483 Our data on the DnaJB8$_{F\rightarrow S}$ mutant illustrate that the JD:CTD interaction exists in the
484 monomeric base unit suggesting that this interaction is present across the polydisperse
485 distribution of DnaJB8 species. Although we as yet lack detailed information supporting
486 a substrate-triggered modulation of the JD:CTD interaction, our results offer some hints
487 toward a possible molecular mechanism for such a coupling. In *in vivo* and *in vitro* XL-MS
488 experiments, negatively charged residues in helix 5 in the G/F domain interact with both
489 the JD and CTD (Fig. 1). We also saw a change in JD:CTD affinity in the absence of the
490 central domains (Fig. 5). Finally, other studies on DnaJB6b have identified the S/T
491 domains as substrate binding domains[16, 20-21]. Future mechanistic and structural studies
492 on DnaJB8 and other complex chaperones including DnaJB6b and their interactions with
493 substrates will reveal the interplay between oligomer dynamics, post-translational

494 modifications, substrate binding, and recruitment of Hsp70.

495

496 **Materials and Methods**

497

498 **Sequence and structural analysis of DnaJB8, DnaJB6b and HspA1A**

499 Analysis of protein sequences (including the net charge per residue; NCPR) was
500 performed using Local CIDER[45]. An ensemble of 1000 HspA1A homology models was
501 produced using *ab initio* Rosetta using the DnaK (PDB:5NRO) conformation as a
502 template[10]. Briefly, the HspA1A sequence was aligned to the DnaK sequence to identify
503 regions with loop insertions and deletions. The HspA1A fragment library was produced
504 using the fragment picker. The lowest scoring model was used to produce a model of the
505 complex between HspA1A and the JD of DnaJB8. The structural images were produced
506 using PyMOL.

507

508 **Cell biological and biochemical analysis of DnaJB8-Clover cell lines**

509 The human *DNAJB8* protein-coding sequence was cloned using Gibson assembly into a
510 modified FM5 lentiviral expression plasmid[46] in which the *UbC* promoter was replaced by
511 a *CMV* promoter, the linker sequence was replaced by "GSAGSAAGSGEF" and
512 the *YFP* was replaced by *mClover3*. The resulting gene produced a DNAJB8-mClover3
513 fusion protein. In parallel, we produced a construct that expresses the fluorescent protein
514 (mClover3) but lacks DnaJB8. Both plasmids we separately co-transfected into HEK293T
515 cells along with helper plasmids (pCMV-VSV-G and psPAX2) to produce lentivirus, which
516 was harvested after 48hrs and used to produce polyclonal cell lines that expressed either
517 DnaJB8-mClover3 or mClover3. For crosslinking experiments, cells from a confluent
518 10cm^2 cell culture dish were pelleted and lysed using an insulin syringe in 1xPBS with
519 1mM DTT, 1mM PMSF, 1x EDTA-free Protease Inhibitor Cocktail (Roche), and 1%
520 Digitonin. After spinning at 1000xg for 10min., the lysate was recovered and incubated
521 with a polyhistidine tagged anti-GFP nanobody (plasmid encoding the nanobody was a
522 kind gift from Dr. Judith Frydman and purified as described previously[24]) for 2.5 hours at
523 4ºC. The lysate was then incubated with 25µL NiNTA beads (Clontech) for 1 hour at 4ºC

524 for binding. The beads were washed five times with 300µL 1xPBS. The buffer for each
525 wash was removed after pulse spinning the beads via centrifugation. The beads were
526 preincubated for 5 minutes at 37ºC and a final concentration of 57mM ADH and 36mM
527 DMTMM were added to each sample. Following a one-minute incubation with chemical
528 crosslinkers, the reaction was quenched with 1mM ammonium bicarbonate. After another
529 pulse spin to remove the buffer, the beads were resuspended in elution buffer, (8M Urea,
530 0.5M imidazole, pH 7.5). After a final pulse spin, the supernatant was retained and
531 analyzed by mass spectrometry.
532
533 **Cross-Linking Reagents**
534 All crosslinking reagents used are commercially available: ADH (Sigma-Aldrich), and
535 mixed light and deuterated ADH (ADH-h_8/d_8) (Creative Molecules). DMTMM (Sigma-
536 Aldrich). For all crosslinking experiments, stock solutions were made of each crosslinking
537 reagent. A 1:1 ADH-d_0/ADH-d_8 solution was made at 100mg/mL in 1xPBS pH 7.4 (Sigma-
538 Aldrich). DMTMM (Sigma-Aldrich) was prepared at a 120mg/mL concentration in 1xPBS
539 pH 7.
540
541 **Cross-Linking Mass Spectrometry**
542 The *ex-vivo* purified DnaJB8 was dialyzed to remove excess imidazole, and transferred
543 into 1xPBS pH 7.4 buffer. For the full-length DnaJB8 experiments, lyophilized DnaJB8
544 was resuspended in either 1xPBS(150mM) or 1xPBS(285mM) to a concentration of
545 100µM. The JD_{1-77} and $CTD_{170-232}$ constructs were purified into 1xPBS buffer, and were
546 prepared for XL-MS experiments at 100µM each. 2µM HspA1A in 1xPBS pH 7.4 buffer
547 and mixed with either 40µM DnaJB8, 40µM JD_{1-77}, 40µM DnaJB8ΔCTD and 40µM
548 $DnaJB8_{F\rightarrow S}$ for XLMS experiments and performed in triplicate. All samples were
549 incubated at 37°C while shaking at 350 rpm for 30 minutes. Final concentrations of 57mM
550 ADH d_o/d_8 (Creative Molecules) and 36mM DMTMM (Sigma-Aldrich) were added to the
551 protein samples and incubated at 37°C with shaking at 350 rpm for 30 minutes. The
552 reactions were quenched with 100mM ammonium bicarbonate and incubated at 37°C for

553 30 min. Samples were lyophilized and resuspended in 8M urea. Samples were reduced
554 with 2.5mM TCEP incubated at 37°C for 30 min followed by alkylation with 5mM
555 iodoacetimide for 30 minutes in the dark. Samples were diluted to 1M urea using a stock
556 of 50mM ammonium bicarbonate and trypsin (Promega) was added at a 1:50 enzyme-to-
557 substrate ratio and incubated overnight at 37°C shaking at 600 rpm. 2% (v/v) formic acid
558 was added to acidify the samples following overnight digestion. All samples were run on
559 reverse phase Sep-Pak tC18 cartridges (Waters) eluted in 50% acetonitrile with 0.1%
560 formic acid. 10µL of the purified peptide fractions was injected for LC-MS/MS analysis on
561 an Eksigent 1D-NanoLC-Ultra HPLC system coupled to a Thermo Orbitrap Fusion Tribrid
562 system. Peptides were separated on self-packed New Objective PicoFrit columns (11cm
563 x 0.075mm I.D.) containing Magic C18 material (Michrom, 3µm particle size, 200Å pore
564 size) at a flow rate of 300nL/min using the following gradient. 0-5min = 5 %B, 5-95min =
565 5-35 %B, 95-97min = 35-95 %B and 97-107min = 95 %B, where A =
566 (water/acetonitrile/formic acid, 97:3:0.1) and B = (acetonitrile/water/formic acid, 97:3:0.1).
567 The mass spectrometer was operated in data dependent mode by selecting the five most
568 abundant precursor ions (m/z 350-1600, charge state 3+ and above) from a preview scan
569 and subjecting them to collision-induced dissociation (normalized collision energy = 35%,
570 30ms activation). Fragment ions were detected at low resolution in the linear ion trap.
571 Dynamic exclusion was enabled (repeat count 1, exclusion duration 30sec).
572
573 **Analysis of Mass Spectrometry Results**
574 All mass spectrometry experiments were carried out on an orbitrap Fusion Lumos Tribrid
575 instrument available through the UTSW proteomics core facility. Each Thermo .raw file
576 was converted to .mzXML format for analysis using an in-house installation of xQuest[47].
577 Score thresholds were set through xProphet[47], which uses a target/decoy model. The
578 search parameters were set as follows. For grouping light and heavy scans (hydrazide
579 crosslinks only): Precursor mass difference for isotope-labeled hydrazides = 8.05021 Da
580 for ADH-d_0/d_8; maximum retention time difference for light/heavy pairs = 2.5 min.
581 Maximum number of missed cleavages = 2, peptide length = 5-50 residues, fixed

582 modifications = carbamidomethyl-Cys (mass shift = 57.02146 Da), mass shift of light
583 crosslinker = 138.09055, mass shift of monolinks = 156.1011 Da, MS^1 tolerance = 15
584 ppm, and MS^2 tolerance = 0.2 Da for common ions and 0.3 Da for crosslink ions; search
585 in enumeration mode. For zero-length crosslink search: maximum number of missed
586 cleavages = 2, peptide length = 5-50 residues, fixed modifications carbamidomethyl-Cys
587 (mass shift = 57.02146 Da), mass shift of crosslinker = -18.010595 Da, no monolink mass
588 specified, MS^1 tolerance = 15 ppm, and MS^2 tolerance = 0.2 Da for common ions and 0.3
589 Da for crosslink ions; search in enumeration mode. The FDRs of all *in vitro* experiments
590 range from 0.05 to 0.33.
591
592 **Western blot analysis**
593 10µL aliquots of the HEK control, Clover, and DnaJB8-Clover cell-lines were removed
594 from the elution and loaded onto a 4-12% Bis-Tris SDS-PAGE gel for western blotting.
595 Upon running the gel to completion, the gel transferred onto a transfer membrane soaked
596 in Novoblot transfer buffer. Following the transfer, the membrane was soaked in milk
597 blocking buffer for 1 hour at room temperature. For immunolabelling, we added 1:2000
598 dilution of polyclonal Anti-GFP (rabbit) (Rockland; 600-401-215; 35460) or Anti-DnaJB8
599 (rabbit) (abcam; ab235546; GR3229943-2) in milk and incubated the membrane shaking
600 at room temperature for 2 hours. The primary antibody solution was dumped and the
601 membrane washed three times for 10 minutes each with 1xTBST before adding the
602 polyclonal Anti-Rabbit IgG Peroxidase (GE Healthcare; NA9340V; 16908235) at a 1:5000
603 dilution in milk. The membrane was incubated with secondary antibody at room
604 temperature for 1 hour before removing the antibody solution. The membrane was
605 washed 3 times in 5-minute intervals with 1xTBST and finally one 5-minute wash with
606 1xTBS. The membrane was soaked in 1mL of Luminol enhancer and peroxide solution
607 for 1 minute before imaging.
608
609 **In cell analysis of DnaJB8-Clover and Clover cell lines**

610 HEK293T cells were treated with 1x and 3x amounts of lentivirus expressing either
611 DnaJB8-mClover3 or mClover alone were plated at 300,000 cells per well in media
612 (10%FBS, 1%Pen/Strep, 1%GlutaMax in DMEM) in a 6-well glass bottom plate (Cellvis,
613 P06-1.5-N). After 30 hours, cells were stained with Hoescht33342 at a final concentration
614 of 2ug/mL in cell media for 30 minutes at 37C and 5%CO2. The plate was placed on an
615 IN Cell 6000 Analyzer (GE Healthcare) with a heated stage and fifty fields of view were
616 imaged under DAPI and FITC channels at 60X magnification (Nikon 60X/0.95, Plan Apo,
617 Corr Collar 0.11-0.23, CFI/60 lambda). Images were exported as TIFF files for
618 downstream analysis. DnaJB8-mClover3, mClover3, and wild-type HEK293 cells were
619 plated and imaged in triplicates. Total cell counting was done using the CellProfiler v3.0
620 software[48] by selecting for DAPI (total cells in acquired images) and mClover3 (total
621 expressing cells in acquired images). Punctae-containing cells were counted manually by
622 two different observers and the data reported as the average with standard deviation
623 between both observers. Expression of Clover and DnaJB8-Clover in 1x and 3x cell lines
624 was quantified from Western blot analysis and by fluorescence intensity of Clover
625 quantified using ImageJ[49].
626
627 **Recombinant expression and purification of DnaJB8 and DnaJB8ΔCTD**
628 The vector used for DnaJB8 expression was a pET-29b vector containing the gene for
629 human DnaJB8, a T7 promoter to activate DnaJB8 expression, a His tag region at the
630 end of the gene, and a gene for kanamycin resistance. The DnaJB8ΔCTD fragment was
631 cloned into pet29b using Gibson assembly. The same protocol was used to express and
632 purify the WT DnaJB8 and DnaJB8ΔCTD proteins. The vector constructs were
633 transformed into *E. coli* BL-21 (DE3) cells and plated onto 2xLB plates containing
634 0.05mg/mL Kanamycin. 12mL of 2xLB, 0.05mg/mL Kanamycin were prepared and
635 inoculated with a single colony from the plate. This small culture was incubated overnight
636 at 37°C while shaking at 220rpm. In the morning, the 12mL culture was added to 1L of
637 2xLB supplemented with 0.05mg/mL Kanomycin and incubated at 37°C while shaking at
638 220rpm. Once OD600 reached 0.6-0.8 A.U., 1mL of 1M IPTG was added to induce

639 DnaJB8 expression. After incubation for an additional 4 hours, the cells were harvested
640 by spinning down the culture at 4,000g for 20 minutes. The resulting cell pellet was
641 resuspended in 25mL 1xPBS and 1mM PMSF in preparation for insoluble fraction
642 separation. The resuspended cells were sonicated at 30% power, 5X pulse for 10 minutes
643 using an Omni Sonic Ruptor 4000 (Omni International). The lysed cells were pelleted at
644 10,000g for 30 minutes and the supernatant was discarded. The insoluble pellet was
645 rinsed with 1xPBS, 0.75%Tween-20 and again pelleted at 10,000g for 30 minutes.
646 The insoluble cell pellet was resuspended in 50mL lysis buffer (8M Guanidinium HCl,
647 50mM HEPES, 20mM Imidazole, 1mM DTT pH 7.5) and sonicated at 30% power, 3X
648 pulse for 1 minute to solubilize the DnaJB8 from the insoluble pellet. After a 30-minute
649 incubation at room temperature, the cellular debris was pelleted at 15,000g for 30
650 minutes. The resulting supernatant was mixed with 2mL HisPur™ Ni-NTA Resin (Thermo
651 Scientific) for 1 hour before being loaded onto a gravity column. The column was washed
652 with an additional 50mL of lysis buffer, followed by 50mL of a second wash buffer (50mM
653 HEPES, 20mM Imidazole, 1mM DTT pH 7.5 in H_2O). The protein was eluted with 30mL
654 of elution buffer (50mM HEPES, 500mM Imidazole, 1mM DTT pH 7.5 in H_2O) and
655 collected in 2mL fractions. After selecting for fractions with high purity, the DnaJB8
656 solution was loaded into 3.5kDa cutoff Biotech CE Dialysis Tubing (Spectrum Labs) and
657 dialyzed overnight at 4ºC in 50mM ammonium formate to minimize assembly. The protein
658 was then lyophilized and stored at -80°C for future use.
659
660 **Dynamic Light Scattering**
661 All samples were prepared at 1.2mg/mL in 1xPBS, 1mM DTT, pH 7.4. All protein samples
662 were filtered through a 0.22µm PES sterile filter and loaded in triplicate onto a 384 well
663 clear flat-bottom plate. The plate was loaded into a Wyatt DynaPro Plate Reader III and
664 set to run continuously at room temperature at a scanning rate of 1 scan per 15 minutes,
665 with 1 scan composed of 10 acquisitions. The data were analyzed using the Wyatt
666 Dynamics software version 7.8.2.18. Light scattering results were filtered by Sum of
667 Squares (SOS) <20 to eliminate statistical outlier acquisitions within each scan. For

668 DnaJB8 in 1xPBS(150mM) buffer, one of the triplicates contains partial data due to high
669 SOS values. This is a result of increasing polydispersity and heterogeneity, which is
670 consistent with oligomers of that size. R_h of observed particles for three time points (0h,
671 10h, and 20h) were reported as histograms as a function of mass%. The mass%
672 contribution of smaller particles in the full-length DnaJB8 runs in 1xPBS(150mM) and
673 (285mM) buffer were reported as a function of mass% over time using the SOS filter and
674 a size filter of <10nm. Data for $DnaJB8_{F\rightarrow S}$, JD_{1-77} and $CTD_{170-232}$ was reported as a
675 function of R_h over time with the SOS filter applied.
676
677 **Modeling of full length DnaJB8 using Rosetta and XL-MS restraints**
678 Given the globular conformations of the JD and CTD we considered how the crosslinks
679 identified for the full-length protein could guide the JD-CTD interaction. Using Rosetta we
680 assembled a monomeric conformation leveraging the JD and CTD conformations while
681 keeping the G/F and S/T regions fully expanded. This starting model was then used in a
682 relax protocol in conjunction with crosslinks (Supplementary Data 1) as constraints to
683 produce an ensemble of 1000 collapsed conformations. A representative low scoring
684 model was selected for further analysis. For acid-acid and acid-lysine contacts 21 and 16
685 Å distance thresholds were used as restraints. The HYDROPRO[50] software was used to
686 calculate radii of hydration from structural models.
687
688 **Conservation mapping**
689 DnaJB8 homolog sequences were identified using Blast[51-52] and the sequences were
690 aligned using Clustal Omega[53]. The protein sequence alignment and structure of DnaJB8
691 JD (PDBID 2DMX) were used as input in Al2Co[54] to map the conservation onto the
692 structural models. The conservation was mapped onto the models in PyMOL.
693
694 **Coevolutionary variation analysis**

695 The GREMLIN software[29-31] was used to identify covarying amino acid pairs from a
696 DnaJB8 protein sequence alignment. A probability of 0.7 was used to threshold the data
697 to identify amino acids with strong coupling.
698

699 **Solid state NMR analysis**

700 Chaperone oligomers were prepared in PBS buffer with different NaCl concentrations.
701 Lyophilized DnaJB8 uniformly labeled with ^{13}C and ^{15}N (U-^{13}C,^{15}N) was re-suspended in
702 1ml of PBS buffer in which the final NaCl concentration was 100mM or 285mM,
703 respectively, for the two samples measured by MAS NMR. Each sample was packed into
704 a 3.2mm MAS NMR rotor (Bruker Biospin) by sedimentation, using a previously described
705 ultracentrifugal packing tool[55] . Sedimentation was done at 175,000 x g force in an Optima
706 L-100 XP Ultracentrifuge using a SW-32 Ti centrifuge rotor for 1 hour. Subsequently,
707 excess of the supernatant fluid was removed. Sample tubes were washed with another
708 1mL buffer solution after which a second packing step using the same parameters was
709 performed. Finally, the supernatant was removed, spacers were placed on the top of the
710 hydrated sedimented protein oligomers, and rotors were closed with the drive cap, and
711 sealed with a small amount of epoxy to avoid sample dehydration.
712

713 Experiments were performed on Bruker 600 MHz and 750 MHz spectrometers, at 277 K
714 temperature using triple-channel (HCN) 3.2mm MAS EFree probes. All experiments were
715 done using TPPM[56] proton decoupling of 83 kHz during acquisition. Single pulse
716 excitation (SPE) measurements were performed using a 6μs 90˚ pulse on ^{13}C, 3s recycle
717 delay, 1k scans and 1D Cross-Polarization experiments (CP) were performed using a
718 3.1μs 90˚ ^{1}H pulse, 2ms contact time, recycle delay of 3s, 1k scans. 1D refocused INEPT
719 experiments were done at using 3μs 90° proton pulse, 4μs 90°pulse on ^{13}C, recycle delay
720 of 2s and 1k scans. The ^{13}C-^{13}C 2D CP-DARR experiments were performed using 25ms
721 mixing time, 0.4ms contact time, 3.1μs 90° proton pulse, 6μs 90°pulse on ^{13}C, recycle
722 delay of 2.8s, 128 scans. The 2D NCA experiment was performed using 3μs 90° proton
723 pulse, 900μs and 3.25ms ^{1}H-^{13}C and ^{13}C-^{15}N contact times respectively, 8μs 180°pulse

724 on ^{15}N, recycle delay of 2s, 576 scans. The amino acid type and secondary structure were
725 predicted using the PLUQ program[38] applied to the chemical shifts in the 2D ^{13}C-^{13}C
726 spectrum. Linewidth analysis was done using the UCSF Sparky NMR analysis program[57].
727 Spectral acquisitions were done with Bruker Topspin software and processing was done
728 with the NMRpipe and Sparky software packages [57-59].
729

730 **Simulations and synthetic NMR spectra**

731 The structure of the DnaJB8 JD in solution was determined previously using solution
732 NMR[42], allowing us also to generate a synthetic ^{13}C-^{13}C 2D spectrum using the
733 corresponding solution NMR chemical shifts from the BMRB (entry 11417). To simulate
734 approximate 2D NMR spectra of the other three domains, we made use of the results of
735 MD simulations of full length DnaJB8. The starting DnaJB8 conformation was produced
736 using ROSETTA with a fully expanded conformation of the G/F and S/T domains while
737 keeping the JD and CTD in the folded conformations. MD simulations were prepared
738 using Maestro[60-61] and carried out in Desmond running the amber99 forcefield. Estimated
739 chemical shifts of the resulting structural models were generated using the SPARTA+
740 package[39].
741

742 **Recombinant Expression and Purification of DnaJB8$_{F\rightarrow S}$, J Domain, and C-Terminal**
743 **Domain**

744 Both vector constructs containing DnaJB8 JD and CTD respectively were cloned into
745 pET-29b using Gibson assembly. The DnaJB8$_{F\rightarrow S}$ construct was purchased from
746 Genscript and cloned into pET-29b. These vectors were transformed into *E. coli* BL-21
747 (DE3) cells and plated onto 2xLB plates with 0.05mg/mL Kanamycin. 12mL of 2xLB with
748 0.05mg/mL Kanamycin were prepared and inoculated with a single colony from each
749 plate. These small cultures were incubated overnight at 37°C while shaking at 220rpm.
750 In the morning, the 12mL culture was added to 1L of 2xLB supplemented with 0.05mg/mL
751 Kanamycin and incubated at 37°C while shaking at 220rpm. Once OD600 reached 0.6-
752 0.8 A.U., 1mL of 1M IPTG was added to induce protein expression. After incubation for

753 an additional 4 hours, the cells were harvested by spinning down the culture at 4,000g for
754 20 minutes. For preparing ^{15}N JD, a single colony was inoculated into 10mL 2xLB
755 supplemented with 0.05mg/mL Kanamycin and incubated for 7-8 hours at 37°C while
756 shaking at 220rpm. The 10mL culture was then mixed into 100mL of M9 minimal media
757 (42mM Na_2HPO_4, 22mM KH_2PO_4, 8.5mM NaCl, 0.1mM CaCl, 2mM Mg_2SO_4, 1E-4%
758 Thiamine, 0.4% Glucose, 187mM NH_4Cl, 0.05mg/mL Kanamycin) and incubated
759 overnight at 37°C while shaking at 220rpm. In the morning of the following day, the cells
760 were spun down at 2,000g for 10minutes and resuspended in 20mLs of M9 minimal media
761 containing 15N labeled NH_4Cl in place of the unlabeled molecule. This was immediately
762 added to 1L of M9 minimal media with ^{15}N labeled NH_4Cl and allowed to incubate at 37°C
763 shaking at 220rpm. Once OD600 reached 0.6-0.8 A.U., 1mL of 1M IPTG was added to
764 induce protein expression. After incubation for an additional 4 hours, the cells were
765 harvested by spinning down the culture at 4,000g for 20 minutes. The cell pellets were
766 resuspended in 20mL of soluble wash buffer (SWB) (50mM KPO_4, 300mM NaCl, 10%
767 glycerol, 1mM PMSF, 10mM BME, pH 8) and sonicated at 30% power, 5X pulse for 10
768 minutes using an Omni Sonic Ruptor 4000 (Omni International). After incubation at room
769 temperature for 1 hour, the cell lysate was spun down at 15,000g for 30 minutes to
770 separate the soluble supernatant from the insoluble pellet. The supernatant was mixed
771 with 2mL TALON® Metal Affinity Resin (Clontech) and incubated shaking at 4°C for 1
772 hour. The protein-resin slurry was loaded onto a gravity column and washed with an
773 additional 40mL of SWB. This was followed by subsequent washes: 20mL SWB with 0.5%
774 tritonX-100, 20mL SWB with adjusted 700mM NaCl, 20mL SWB with 0.1mM ATP and
775 5mM $MgCl_2$, and an additional 40mL of SWB. The protein was eluted with 16mL SWB
776 with 200mM Imidazole into 2mL fractions. After selecting for fractions with high purity, the
777 protein solution was loaded into 3.5kDa cutoff Biotech CE Dialysis Tubing (Spectrum
778 Labs) and dialyzed overnight at 4°C in 1xPBS to restore native folding. Both domain
779 constructs were further enriched by running on a GE Superdex 200 Increase 10/300
780 column in 1xPBS 1mM DTT pH 7. The protein was aliquoted and flash frozen in liquid
781 nitrogen and stored at -80°C for future use.

782

783 **SEC-MALS**

784 DnaJB8$_{F\rightarrow S}$, JD$_{1-77}$, and CTD$_{170-232}$ constructs at a concentration of 5.1 mg/mL, 5.0
785 mg/mL, and 6.6 mg/mL, respectively, in 1xPBS were filtered through a 0.1 µm filter to
786 remove larger impurities. Each sample was further filtered using a 0.22 µm centrifugal
787 filter before 100 µL was applied to a Superdex 200 Increase 10/300 column equilibrated
788 in 1xPBS. The column was in line with a Shimadzu UV detector, a Wyatt TREOS II light-
789 scattering detector, and a Wyatt Optilab tREX differential-refractive-index detector. The
790 flow rate was 0.5 mL/min. The data were analyzed with Wyatt's ASTRA software version
791 7.1.0.29. SEDFIT[62] was used to calculate the dn/dc of the protein.

792

793 **Circular Dichroism**

794 Recombinant CTD$_{170-232}$ domain constructs were transferred into 10mM $NaPO_4$, 150mM
795 NaF, pH 7.4 buffer at a concentration of 40µM. The experiment was run using a Jasco J-
796 815 Circular Dichroism instrument with a PMT detector using a 10 mm quartz cuvette. 6
797 accumulations were taken at a speed of 50 nm/min along the UV spectrum from 190 nm
798 to 300 nm. Spectra analysis was done using the BeStSel online software[63-64] to determine
799 secondary structural composition.

800

801 **CTD model generation**

802 Fragment libraries for the CTD sequence were generated using the Robetta server. 5000
803 models were produced using the *ab initio* protocol and clustered to identify unique
804 conformations. Lowest scoring models from the top clusters showed high structural
805 similarity. The identified crosslinks from the CTD in full length DnaJB8 or isolated CTD
806 were evaluated for consistency with each model in the ensemble. For acid-acid and acid-
807 lysine crosslinks a distance threshold of 21 and 16 Å, respectively, was considered as
808 satisfied and consistent with the chemistry. Distances were calculated using a custom
809 script in MATLAB ver.R2019a and the crosslink pairs were visualized using PyMOL. The
810 HYDROPRO[50] software was used to calculate radii of hydration from structural models.

811

812 **Fluorescence polarization**

813 JD_{1-77} was labelled with 10x FITC-maleimide (sigma) in 1xPBS 1mM TCEP for 2 hours at
814 room temperature. The reaction was quenched and the excess dye was removed using
815 a Zeba spin desalting column (Thermo). For all experiments, 0.2µM JD_{1-77} was incubated
816 in triplicate with a titration gradient of Hsp70 (150µM-0µM) or $CTD_{170-232}$(150µM-0µM) in
817 1xPBS, 1mM TCEP, pH 7.4. For competition experiments, labelled JD_{1-77} was mixed with
818 3.125µM CTD in triplicate and incubated at room temperature for 1 hour before adding a
819 titration gradient of Hsp70(150µM-0µM). Fluorescence polarization readings were taken
820 with excitation at 494nm and emission at 525nm. The data were fit to a one site specific
821 binding model using GraphPad Prism 7.04.

822

823 **Microscale Thermophoresis**

824 The MST binding experiments were performed on Nanotemper Monolith NT.115 in the
825 Molecular Biophysics Resource core at UTSW and analyzed with a standard protocol[65].
826 Binding measurements were performed in triplicate. The JD_{1-77} was labeled with FITC-
827 maleimide (sigma) and 200nM JD_{1-77}-FITC was titrated by a serial 2-fold dilution of
828 $CTD_{180-232}$. Data were fit in PALMIST[65] to a 1:1 binding model.

829

830

831 **Solution NMR with ^{15}N-labeled JD and CTD**

832 The 300µM ^{15}N-labeled JD was exchanged into 20mM Tris 100mM NaCl 1mM DTT pH 7
833 buffer in preparation for solution NMR. Each HSQC run was done for 4 hours at 1
834 scans/min with the temperature fixed at 299K. After each run, unlabeled CTD was titrated
835 into the sample at 1:1, 1:3, and 1:6 ratios sequentially. All scans were collected on an
836 Agilent DD2 600MHz instrument at the UT Southwestern Biomolecular NMR Facility.
837 Each spectrum was converted into a readable format and phase corrected using
838 NMRPipe[58]. Peak assignments were based on the deposited information from BMRB
839 (11417). The software Sparky[57, 59] was used to analyze the peak shifts across all spectra.

840

841

842 **Recombinant expression and purification of HspA1A**

843 HspA1A gene was cloned into the pMCSG7 plasmid[66] and transformed into BL-21 (DE3)
844 cells and plated onto 2xLB plates with 0.1mg/mL ampicillin. 12mL of 2xLB with 0.1mg/mL
845 ampicillin were prepared and inoculated with a single colony from each plate. These small
846 cultures were incubated overnight at 37ºC while shaking at 220rpm. In the morning, the
847 12mL culture was added to 1L of 2xLB supplemented with 0.1mg/mL ampicillin and
848 incubated at 37°C while shaking at 220rpm. Once OD600 reached 0.6-0.8 A.U., 1mL of
849 1M IPTG was added to induce protein expression. The cells continued to incubate
850 overnight at 12ºC shaking at 220rpm. After incubation, the cells were lysed using a
851 PandaPlus 2000 homogenizer (GEA) by pressing the cells with 10,000p.p.m pressure.
852 The lysate was spun at 15,000xg for 45 minutes to remove insoluble cell components,
853 and the resulting supernatant was mixed with 2mL TALON® Metal Affinity Resin
854 (Clontech) and incubated at 4ºC for 1 hour. The slurry was spun down at 700xg for 2 min
855 to remove the majority of the buffer and the beads were added onto a gravity column. The
856 beads were washed with 6CV of wash buffer (50mM Tris, 500mM NaCl, 10mM imidazole,
857 5mM βME, pH 8) and eluted with 5mL of elution buffer (50mM Tris, 500mM NaCl, 300mM
858 imidazole, 5mM βME, pH 8). HspA1A containing fractions were confirmed by SDS-PAGE
859 and pooled together for desalting. Desalting/buffer exchange was performed using a PD-
860 10 desalting column (GE Healthcare), where HspA1A fractions were transferred into
861 anion-exchange wash buffer (50mM Tris, 20mM NaCl, 1mM DTT, pH 8.75). The protein
862 was loaded onto a HiTrap Q HP anion exchange column (GE Healthcare) and eluted
863 across a gradient of anion-exchange elution buffer (50mM Tris, 1M NaCl, 1mM DTT, pH
864 8.75). HspA1A-containing fractions were once again combined and loaded onto a
865 Superdex™ 200 Increase 10/300 GL (GE Life Sciences) size exclusion column, where
866 HspA1A was further purified and transferred into 1xPBS, 1mM DTT, pH 7.4 buffer for all
867 subsequent experiments.

868

869 **Acknowledgements**

This work was supported by grants from the Welch Foundation and the Effie Marie Cain Endowed Scholarship (L.A.J.) and NIGMS R01 GM112678 (P.V.D.W.). We appreciate the help of the Molecular Biophysics Resource core, Structural Biology Laboratory, Biomolecular Nuclear Magnetic Resonance Facility, and Proteomics Core Facility at the University of Texas Southwestern Medical Center. The 750 MHz ssNMR instrument at the University of Pittsburgh was acquired with funding from NIH grant 10 OD012213-01.

Author Contributions

B.D.R., I.M., P.V.D.W., and L.A.J. conceived and designed the overall study. B.D.R. performed *in vitro* protein binding assays, cell models, crosslink mass spectrometry, and ROSETTA simulations. I.M. and P.V.D.W. performed ssNMR experiments and analyzed the data. S.B. performed DnaJB8 CTD experiments and ROSETTA simulations. J.V.A produced mammalian cell lines and collected microscopy images. B.D.R., I.M., P.V.D.W., and L.A.J. wrote the manuscript, and all authors contributed to its improvement.

Competing Interests

The authors declare no competing interests.

Data availability

The data sets generated during and/or analysed during the current study are available from the corresponding authors on reasonable request.

References

1. Minami, Y.; Hohfeld, J.; Ohtsuka, K.; Hartl, F. U., Regulation of the heat-shock protein 70 reaction cycle by the mammalian DnaJ homolog, Hsp40. *J Biol Chem* **1996,** *271* (32), 19617-24.

900 2. Wall, D.; Zylicz, M.; Georgopoulos, C., The NH2-terminal 108 amino acids of the
901 Escherichia coli DnaJ protein stimulate the ATPase activity of DnaK and are sufficient for lambda
902 replication. *J Biol Chem* **1994,** *269* (7), 5446-51.
903 3. Wall, D.; Zylicz, M.; Georgopoulos, C., The conserved G/F motif of the DnaJ chaperone is
904 necessary for the activation of the substrate binding properties of the DnaK chaperone. *J Biol*
905 *Chem* **1995,** *270* (5), 2139-44.
906 4. Hartl, F. U., Molecular chaperones in cellular protein folding. *Nature* **1996,** *381* (6583),
907 571-9.
908 5. Cheetham, M. E.; Caplan, A. J., Structure, function and evolution of DnaJ: conservation
909 and adaptation of chaperone function. *Cell Stress Chaperones* **1998,** *3* (1), 28-36.
910 6. Muchowski, P. J.; Wacker, J. L., Modulation of neurodegeneration by molecular
911 chaperones. *Nat Rev Neurosci* **2005,** *6* (1), 11-22.
912 7. Kampinga, H. H.; Craig, E. A., The HSP70 chaperone machinery: J proteins as drivers of
913 functional specificity. *Nat Rev Mol Cell Biol* **2010,** *11* (8), 579-92.
914 8. Ahmad, A.; Bhattacharya, A.; McDonald, R. A.; Cordes, M.; Ellington, B.; Bertelsen, E. B.;
915 Zuiderweg, E. R. P., Heat shock protein 70 kDa chaperone/DnaJ cochaperone complex employs
916 an unusual dynamic interface. *Proc Natl Acad Sci U S A* **2011,** *108*, 18966-18971.
917 9. Flaherty, K. M.; DeLuca-Flaherty, C.; McKay, D. B., Three-dimensional structure of the
918 ATPase fragment of a 70K heat-shock cognate protein. *Nature* **1990,** *346* (6285), 623-8.
919 10. Kityk, R.; Kopp, J.; Mayer, M. P., Molecular Mechanism of J-Domain-Triggered ATP
920 Hydrolysis by Hsp70 Chaperones. *Mol Cell* **2018,** *69* (2), 227-237 e4.
921 11. Rampelt, H.; Kirstein-Miles, J.; Nillegoda, N. B.; Chi, K.; Scholz, S. R.; Morimoto, R. I.;
922 Bukau, B., Metazoan Hsp70 machines use Hsp110 to power protein disaggregation. *EMBO J*
923 **2012,** *31* (21), 4221-35.
924 12. Wagner, I.; Arlt, H.; van Dyck, L.; Langer, T.; Neupert, W., Molecular chaperones
925 cooperate with PIM1 protease in the degradation of misfolded proteins in mitochondria. *EMBO*
926 *J* **1994,** *13* (21), 5135-45.
927 13. Nakatsukasa, K.; Huyer, G.; Michaelis, S.; Brodsky, J. L., Dissecting the ER-associated
928 degradation of a misfolded polytopic membrane protein. *Cell* **2008,** *132* (1), 101-12.
929 14. Nillegoda, N. B.; Stank, A.; Malinverni, D.; Alberts, N.; Szlachcic, A.; Barducci, A.; De Los
930 Rios, P.; Wade, R. C.; Bukau, B., Evolution of an intricate J-protein network driving protein
931 disaggregation in eukaryotes. *Elife* **2017,** *6*.
932 15. Jiang, Y.; Possi, P.; Kalodimos, C. G., Structural basis for client recognition and activity of
933 Hsp40 chaperones. *Science* **2019,** *365* (6459), 1313-1319.
934 16. Hageman, J.; Rujano, M. A.; van Waarde, M. A.; Kakkar, V.; Dirks, R. P.; Govorukhina, N.;
935 Oosterveld-Hut, H. M.; Lubsen, N. H.; Kampinga, H. H., A DNAJB chaperone subfamily with
936 HDAC-dependent activities suppresses toxic protein aggregation. *Mol Cell* **2010,** *37* (3), 355-69.
937 17. Karamanos, T. K.; Tugarinov, V.; Clore, G. M., Unraveling the structure and dynamics of
938 the human DNAJB6b chaperone by NMR reveals insights into Hsp40-mediated proteostasis.
939 *Proc Natl Acad Sci U S A* **2019**.
940 18. Månsson, C.; Kakkar, V.; Monsellier, E.; Sourigues, Y.; Härmark, J.; Kampinga, H. H.;
941 Melki, R.; Emanuelsson, C., DNAJB6 is a peptide-binding chaperone which can suppress amyloid

942 fibrillation of polyglutamine peptides at substoichiometric molar ratios. *Cell Stress and*
943 *Chaperones* **2014,** *19*, 227-239.
944 19. Söderberg, C. A. G.; Månsson, C.; Bernfur, K.; Rutsdottir, G.; Härmark, J.; Rajan, S.; Al-
945 Karadaghi, S.; Rasmussen, M.; Höjrup, P.; Hebert, H.; Emanuelsson, C., Structural modelling of
946 the DnaJB6 oligomeric chaperone shows a peptide-binding cleft lined with conserved S/T-
947 residues at the dimer interface. *Scientific Reports* **2018,** *8* (5199).
948 20. Gillis, J.; Schipper-Krom, S.; Juenemann, K.; Gruber, A.; Coolen, S.; van den Nieuwendijk,
949 R.; van Veen, H.; Overkleeft, H.; Goedhart, J.; Kampinga, H. H.; Reits, E. A., The DNAJB6 and
950 DNAJB8 protein chaperones prevent intracellular aggregation of polyglutamine peptides. *J Biol*
951 *Chem* **2013,** *288* (24), 17225-37.
952 21. Kakkar, V.; Mansson, C.; de Mattos, E. P.; Bergink, S.; van der Zwaag, M.; van Waarde,
953 M. A.; Kloosterhuis, N. J.; Melki, R.; van Cruchten, R. T.; Al-Karadaghi, S.; Arosio, P.; Dobson, C.
954 M.; Knowles, T. P.; Bates, G. P.; van Deursen, J. M.; Linse, S.; van de Sluis, B.; Emanuelsson, C.;
955 Kampinga, H. H., The S/T-Rich Motif in the DNAJB6 Chaperone Delays Polyglutamine
956 Aggregation and the Onset of Disease in a Mouse Model. *Mol Cell* **2016**.
957 22. Shahmoradian, S. H.; Galez-Montoya, J. G.; Schmid, M. F.; Cong, Y.; Ma, B.; Spiess, C.;
958 Frydman, J.; Ludtke, S. J.; Chiu, W., TRiC's tricks inhibit huntingtin aggregation. *eLife* **2013,** *2*
959 (e00710).
960 23. Kirchhofer, A.; Helma, J.; Schmidthals, K.; Frauer, C.; Cui, S.; Karcher, A.; Pellis, M.;
961 Muyldermans, S.; Casas-Delucchi, C. S.; Cardoso, M.; Leonhardt, H.; Hopfner, K. P.; Rothbauer,
962 U., Modulation of protein properties in living cells using nanobodies. *Nat. Struc. and Mol. Bio.*
963 **2010,** *17* (1), 133-138.
964 24. Kubala, M. H.; Kovtun, O.; Alexandrov, K.; Collins, B. M., Structural and thermodynamic
965 analysis of the GFP:GFP-nanobody complex. *Protein Sci.* **2010,** *19* (12), 2389-2401.
966 25. Leitner, A.; Faini, M.; Stengel, F.; Aebersold, R., Crosslinking and Mass Spectometry: An
967 Integrated Technology to Understand the Structure and Function of Molecular Machines. *Cell*
968 *Press* **2016,** *41* (1), 20-32.
969 26. Leitner, A.; Joachimiak, L. A.; Unverdorben, P.; Walzthoeni, T.; Frydman, J.; Förster, F.;
970 Aebersold, R., Chemical cross-linking/mass spectometry targeting acidic residues in proteins
971 and protein complexes. *Proc Natl Acad Sci U S A* **2014,** *111* (26), 9455-9460.
972 27. Walzthoeni, T.; Joachimiak, L. A.; Rosenberger, G.; Röst, H. L.; Malmström, L.; Leitner, A.;
973 Frydman, J.; Aebersold, R., xTract: software for characterizing conformational changes of
974 protein complexes by quantitative cross-linking mass spectometry. *Nat Methods* **2015,** *12* (12),
975 1185-1190.
976 28. Månsson, C.; Arosio, P.; Hussein, R.; Kampinga, H. H.; Hashem, R. M.; Boelens, W. C.;
977 Dobson, C. M.; Knowles, T. P.; Linse, S.; Emanuelsson, C., Interaction of the molecular
978 chaperone DNAJB6 with growing amyloid-beta 42 (Abeta42) aggregates leads to sub-
979 stoichiometric inhibition of amyloid formation. *J Biol Chem* **2014,** *289* (45), 31066-76.
980 29. Ovchinnikov, S.; Kamisetty, H.; Baker, D., Robust and accurate prediction of residue-
981 residue interactions across protein interfaces using evolutionary information. *Elife* **2014,** *3*.
982 30. Kamisetty, H.; Ovchinnikov, S.; Baker, D., Assessing the utility of coevolution-based
983 residue-residue contact predictions in a sequence- and structure-rich era. *Proc Natl Acad Sci U S*
984 *A* **2013,** *110* (39), 15674-15679.

31. Balakrishnan, S.; Kamisetty, H.; Carbonell, J. G.; Lee, S.; Langmead, C. J., Learning generative models for protein fold families. *Proteins: Structure, Function, and Bioinformatics* **2011,** *79* (4), 1061-1078.
32. Marsh, J. A.; Forman-Kay, J. D., Sequence determinants of compaction in intrinsically disordered proteins. *Biophys. J.* **2010,** *98*, 2383-2390.
33. Matlahov, I.; van der Wel, P. C. A., Hidden motions and motion-induced invisibility: Dynamics-based spectral editing in solid-state NMR. *Methods* **2018,** *148*, 123-135.
34. Morris, G. A.; Freeman, R., Enhancement of Nuclear Magnetic-Resonance Signals by Polarization Transfer. *J Am Chem Soc* **1979,** *101* (3), 760-762.
35. Lin, H. K.; Boatz, J. C.; Krabbendam, I. E.; Kodali, R.; Hou, Z. P.; Wetzel, R.; Dolga, A. M.; Poirier, M. A.; van der Wel, P. C. A., Fibril polymorphism affects immobilized non-amyloid flanking domains of huntingtin exon1 rather than its polyglutamine core. *Nat Commun* **2017,** *8*.
36. Andronesi, O. C.; Becker, S.; Seidel, K.; Heise, H.; Young, H. S.; Baldus, M., Determination of Membrane Protein Structure and Dynamics by Magic-Angle-Spinning Solid-State NMR Spectroscopy. *J. Am. Chem. Soc.* **2005,** *127* (37), 12965-12974.
37. Fritzsching, K. J.; Hong, M.; Schmidt-Rohr, K., Conformationally selective multidimensional chemical shift ranges in proteins from a PACSY database purged using intrinsic quality criteria. *J Biomol NMR* **2016,** *64* (2), 115-30.
38. Fritzsching, K. J.; Yang, Y.; Schmidt-Rohr, K.; Hong, M., Practical use of chemical shift databases for protein solid-state NMR: 2D chemical shift maps and amino-acid assignment with secondary-structure information. *J Biomol NMR* **2013,** *56* (2), 155-67.
39. Shen, Y.; Bax, A., SPARTA+: a modest improvement in empirical NMR chemical shift prediction by means of an artificial neural network. *J Biomol NMR* **2010,** *48* (1), 13-22.
40. Mandal, A.; Hoop, C. L.; DeLucia, M.; Kodali, R.; Kagan, V. E.; Ahn, J.; van der Wel, P. C. A., Structural Changes and Proapoptotic Peroxidase Activity of Cardiolipin-Bound Mitochondrial Cytochrome c. *Biophys. J.* **2015,** *109*, 1873-1884.
41. Qi, R.; Sarbeng, E. B.; Liu, Q.; Le, K. Q.; Xu, X.; Xu, H.; Yang, J.; Wong, J. L.; Vorvis, C.; Hendrickson, W. A.; Zhou, L.; Liu, Q., Allosteric opening of the polypeptide-binding site when an Hsp70 binds ATP. *Nat. Struct. Mol. Biol.* **2013,** *20*, 900-907.
42. Ohnishi, S.; Tochio, N.; Koshiba, S.; Inoue, M.; Kigawa, T.; Yokoyama, S., Solution structure of the J domain of DnaJ homolog subfamily B member 8. RIKEN Structural Genomics/Proteomics Initiative (RSGI), 2006.
43. Mayer, M. P.; Laufen, T.; Paal, K.; McCarty, J. S.; Bukau, B., Investigation of the interaction between DnaK and DnaJ by surface plasmon resonance spectroscopy. *J Mol Biol* **1999,** *289* (4), 1131-1134.
44. Martin, E. W.; Holehouse, A. S.; Peran, I.; Farag, M.; Incicco, J. J.; Bremer, A.; Grace, C. R.; Sorano, A.; Pappu, R. V.; Mittag, T., Valence and Patterning of Aromatic Residues Determine the Phase Behavior of Prion-Like Domains. *Science* **2020,** *367* (6478), 694-699.
45. Holehouse, A. S.; Ahad, J.; Das, R. K.; Pappu, R. V., CIDER: Classification of Intrinsically Disordered Ensemble Regions. *Biophys. J.* **2015,** *108*, 228a.
46. Sanders, D. W.; Kaufman, S. K.; DeVos, S. L.; Sharma, A. M.; Mirbaha, H.; Li, A.; Barker, S. J.; Foley, A.; Thorpe, J. R.; Serpell, L. C.; Miller, T. M.; Grinberg, L. T.; Seeley, W. W.; Diamond, M.

1027 I., Distinct tau prion strains propagate in cells and mice and define different tauopathies.
1028 *Neuron* **2014,** *82* (6), 1271-1288.
1029 47. Leitner, A.; Walzthoeni, T.; Aebersold, R., Lysine-specific chemical cross-linking of
1030 protein complexes and identification of cross-linking sites using LC-MS/MS and the
1031 xQuest/xProphet software pipeline. *Nat. Protocols* **2014,** *9*, 120-137.
1032 48. McQuin, C.; Goodman, A.; Chernyshev, V.; Kamentsky, L.; Cimini, B. A.; Karhohs, K. W.;
1033 Doan, M.; Ding, L.; Rafelski, S. M.; Thirstrup, D.; Wiegraebe, W.; Singh, S.; Becker, T.; Caicedo, J.
1034 C.; Carpenter, A. E., CellProfiler 3.0: Next-generation image processing for biology. *PLoS Biol.*
1035 **2018,** *16* (7), e2005970.
1036 49. Schneider, C. A.; Rasband, W. S.; Eliceiri, K. W., NIH Image to ImageJ: 25 years of image
1037 analysis. *Nat. Methods* **2012,** *9*, 671-675.
1038 50. Ortega, A.; Amoros, D.; Garcia, J., Prediction of hydrodynamic and other solution
1039 properties of rigid proteins from atomic and residue-level models. *Biophys. J.* **2011,** *101*, 892-
1040 898.
1041 51. Altschul, S. F.; Gish, W.; Miller, W.; Myers, E. W.; Lipman, D. J., Basic Local Alignment
1042 Search Tool. *J. Mol. Bio.* **1990,** *215*, 403-410.
1043 52. Altschul, S. F.; Madden, T. L.; Schäffer, A. A.; Zhang, Z.; Miller, W.; Lipman, D. J., Gapped
1044 BLAST and PSI-BLAST: a new generation of protein database search programs. *Nucleic Acids*
1045 *Research* **1997,** *25*, 3389-3402.
1046 53. Madeira, F.; Park, Y. M.; Lee, J.; Buso, N.; Gur, T.; Madhusoodanan, N.; Basutkar, P.;
1047 Tivey, A. R. N.; Potter, S. C.; Finn, R. D.; Lopez, R., The EMBL-EBI search and sequence analysis
1048 tools APIs in 2019. *Nucleic Acids Research* **2019,** *47* (W1), 636-641.
1049 54. Pei, J.; Grishin, N. V., AL2CO: calculation of positional conservation in a protein sequence
1050 alignment. *Bioinformatics* **2001,** *17* (8), 700-712.
1051 55. Mandal, A.; Boatz, J. C.; Wheeler, T. B.; van der Wel, P. C., On the use of ultracentrifugal
1052 devices for routine sample preparation in biomolecular magic-angle-spinning NMR. *J Biomol*
1053 *NMR* **2017,** *67* (3), 165-178.
1054 56. Bennett, A. E.; Rienstra, C. M.; Auger, M.; Lakshmi, K. V.; Griffin, R. G., Heteronuclear
1055 Decoupling in Rotating Solids. *J Chem Phys* **1995,** *103* (16), 6951-6958.
1056 57. D., G. T.; G., K. D. *SPARKY 3*, 3.110; University of California, San Francisco: San Francisco,
1057 CA, 2004.
1058 58. Delaglio, F.; Grzesiek, S.; Vuister, G. W.; Zhu, G.; Pfeifer, J.; Bax, A., NMRPipe: A
1059 multidimensional spectral processing system based on UNIX pipes. *Journal of Biomolecular*
1060 *NMR* **1995,** *6*, 277-293.
1061 59. Lee, W.; Tonelli, M.; Markley, J. L., NMRFAM-SPARKY: enhanced software for
1062 biomolecular NMR spectroscopy. *Bioinformatics* **2015,** *31* (8), 1325-1327.
1063 60. *Schrödinger Release 2019-3*, D.E. Shaw Research: New York, NY, 2019.
1064 61. Bowers, K. J.; Chow, E.; Xu, H.; Dror, R. O.; Eastwood, M. P.; Gregersen, B. A.; Klepeis, J.
1065 L.; Kolossvary, I.; Moraes, M. A.; Sacerdoti, F. D.; Salmon, J. K.; Shan, Y.; Shaw, D. E. In *Scaleable*
1066 *Algorithms for Molecular Dynamics Simulations on Commodity Clusters*, Proceedings of the
1067 ACM/IEEE Conference on Supercomputing (SC06), Tampa, FL, November 11-17; ACM: Tampa,
1068 FL, 2006.

1069 62. Schuck, P., Size-distribution Analysis of Macromolecules by Sedimentation Veelocity
1070 Ultracentrifugation and Lamm Equation Modeling. *Biophys. J.* **2000,** *78* (3), 1606-1619.
1071 63. Micsonai, A.; Wien, F.; Bulyáki, E.; Kun, J.; Moussong, E.; Lee, Y.; Goto, Y.; Réfrégiers, M.;
1072 Kardos, J., BeStSel: a web server for accurate protein secondary structure predicition and fold
1073 recognition from the circular dichroism spectra. *Nucleic Acids Research* **2018,** *46* (W), 315-322.
1074 64. Micsonai, A.; Wien, F.; Kernya, L.; Lee, Y.; Goto, Y.; Réfrégiers, M.; Kardos, J., Accurate
1075 scondary structure prediction and fold recognition for circular dichroism spectroscopy. *Proc*
1076 *Natl Acad Sci U S A* **2015**.
1077 65. Scheuermann, T. H.; Padrick, S. B.; Gardner, K. H.; Brautigam, C. A., On the acquisition
1078 and analysis of microscale thermophoresis data. *Anal Biochem.* **2016,** *496*, 79-93.
1079 66. Eschenfeldt, W. H.; Lucy, S.; Millard, C. S.; Joachimiak, A.; Mark, I. D., A family of LIC
1080 vectors for high-throughput cloning and purification of proteins. *Methods Mol. Biol.* **2009,** *498*,
1081 105-115.
1082

1083

1084

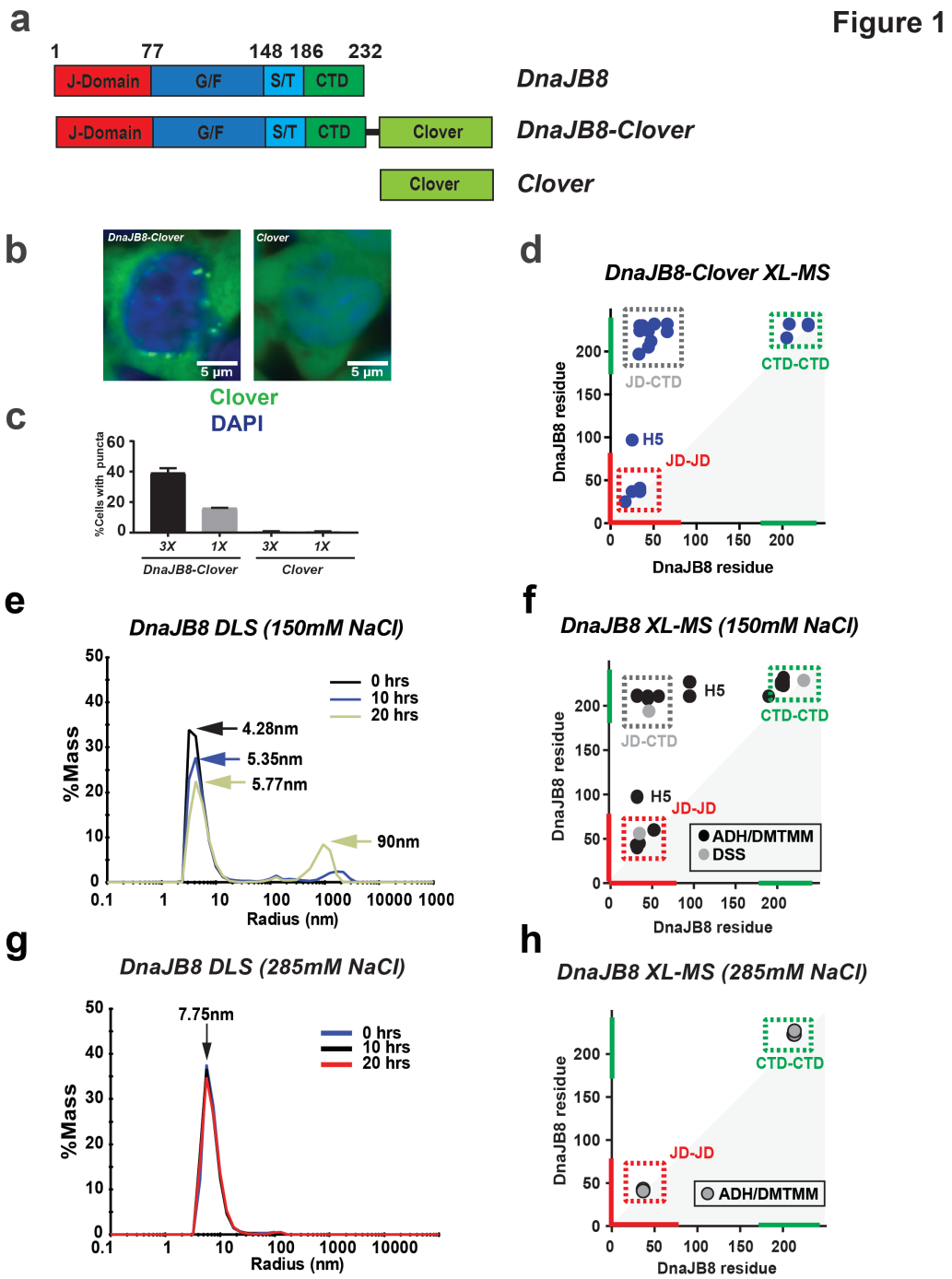

Figure 1. DnaJB8 architecture defined by domain-domain interactions. (**a**) Domain maps for DnaJB8 used in the *in vitro* experiments and the DnaJB-Clover and Clover constructs used in the mammalian cell experiments. DnaJB8 colored according to domain annotation: JD (red), G/F rich (blue), S/T rich (cyan), and CTD (green). Clover is colored pale green. (**b**) Representative images of triplicate populations of 300,000 cells expressing DnaJB8-mClover3(left) and mClover3(right). Clover and DAPI fluorescence signal are shown in green and blue, respectively. 5µm scale bar is shown in white. (**c**) Quantification of DnaJB8-Clover and Clover puncta in high (3X) and low (1X)

protein level expressing cell lines. In each analysis at least 2,000 cells were counted by the CellProfiler software. Puncta were manually counted by two independent observers, with data reported as averages with standard deviation. (**d**) XL-MS contact map of DnaJB8-Clover crosslinks identified using DMTMM and ADH. The axes are colored in red and green for JD and CTD, respectively. Crosslink pairs between JD-CTD, JD-JD and CTD-CTD are shown in dashed boxes colored grey, red and green, respectively. Contacts to helix 5 are denoted with H5. (**e)** Histogram of overall R_h of DnaJB8 in 1xPBS 150mM NaCl from DLS at times 0hrs (black), 10hrs (blue), and 20hrs (gold) with arrows indicating R_h peaks for each time point. Over time, there was a depletion in particle sizes <10nm and an increase in particles ~100-1000nm. **(f)** XL-MS contact map of DnaJB8 crosslinks identified using DMTMM and ADH (black) and DSS (grey). The axes are colored in red and green for JD and CTD, respectively. Crosslink pairs between JD-CTD, JD-JD and CTD-CTD are shown in a dashed box colored grey, red and green, respectively. Contacts to helix 5 are denoted with H5. **(g**) Histogram of overall R_h of DnaJB8 in 1xPBS 285mM NaCl at times 0h (blue), 10h (black), and 20h (red) with arrows indicating R_h peaks for each time point. Over time, there is no change in the species of particle sizes <10nm and no appearance of particles ~100-1000nm. **(h)** Contact map of DnaJB8 crosslinks identified using ADH/DMTMM in the presence of 285mM NaCl. The axes are colored in red and green for JD and CTD, respectively. JD-JD and CTD-CTD crosslinks are shown in dashed boxes colored in red and green, respectively.

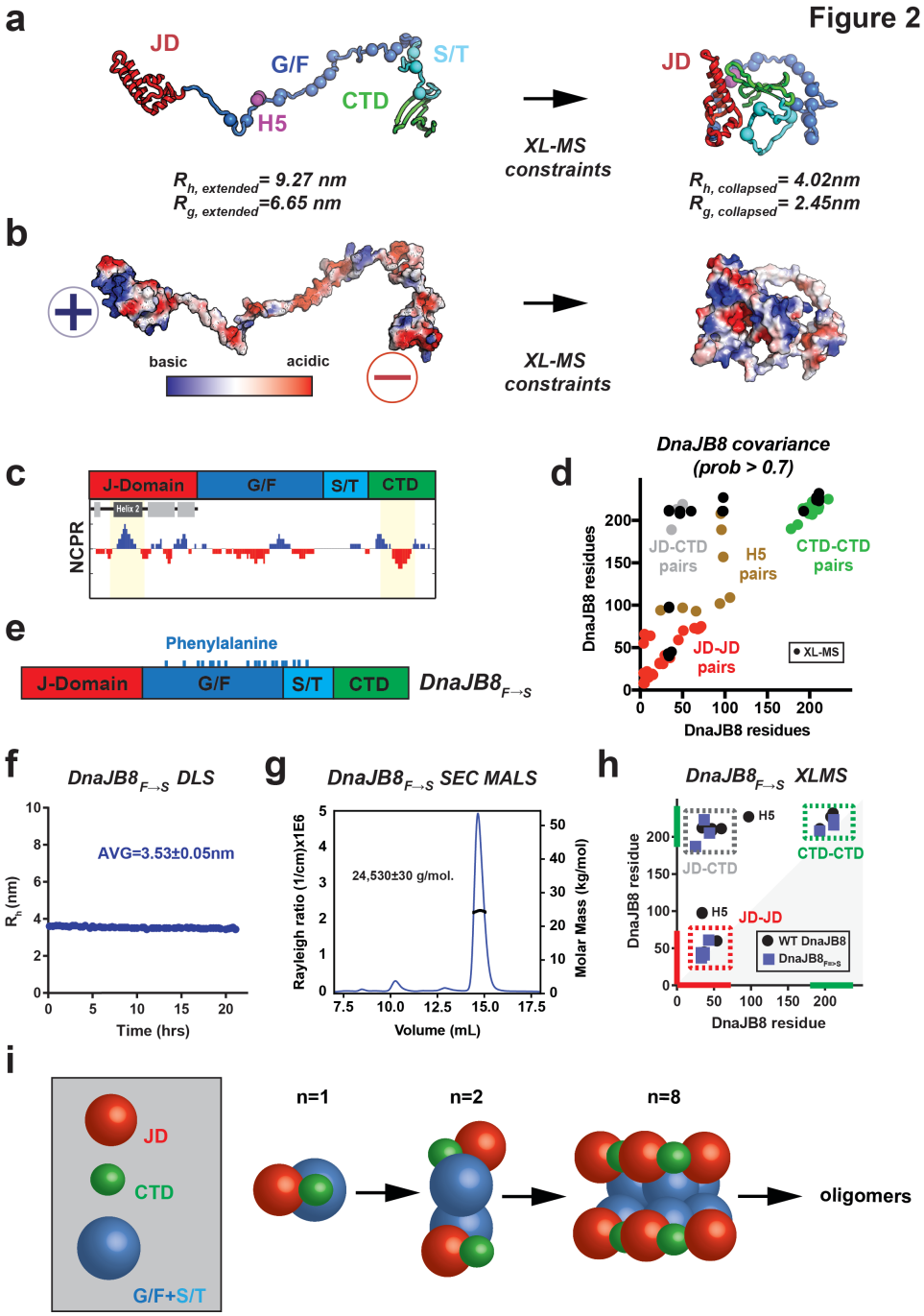

Figure 2. Model for the JD-CTD contacts in a DnaJB8 monomer. (**a**) XL-MS-based refinement of full length expanded DnaJB8 monomer. Cartoon representation of DnaJB8 in fully expanded conformation (left) and collapsed conformation (right), colored by domain as in Fig. 1. Aromatic amino acids in the G/F and S/T domains are shown as spheres and colored according to the domain. Residues in helix 5 (H5) are shown as magenta spheres. Collapsed conformation model was selected from 1,000 Rosetta *ab initio* generated models using a relax protocol. R_g and R_h values were calculated from the structural model in Rosetta and HYDROPRO, respectively. (**b**)

Charge complementary surfaces on the JD and CTD mediate the interaction. Highly acidic potential is shown in red (- sign) and highly basic in blue (+ sign). **(c)** Net charge per residue (NCPR) distribution, defined as the average charge over a 10-residue window, highlights charge complementarity between basic and acidic residues on the JD and CTD, respectively (coloring as in Fig. 1). **(d)** GREMLIN sequence-based covariance analysis identified high confidence covarying amino acids on DnaJB8 that localize within the JD (red), within CTD (green), with H5 (brown) and across JD-CTD (grey). XL-MS links for full length DnaJB8 (black dots) overlap with the covarying regions. Covarying positions localizing to amino acids in G/F domain are shown in brown and co-localize with XL-MS crosslinks. **(e)** Domain map of the DnaJB8$_{F\rightarrow S}$ mutant, with mutated phenylalanine positions marked by cyan ticks. **(f)** DLS time course of the DnaJB8$_{F\rightarrow S}$ mutant. The average R_h was calculated to be 3.53±0.05nnm. **(g)** SEC-MALS of CTD$_{170\text{-}232}$ shows a single peak that was calculated to have a molar mass of 24,530±30 g/mol consistent with a monomer. **(h)** XL-MS contact map showing ADH/DMTMM crosslinks for WT DnaJB8 and DnaJB8$_{F\rightarrow S}$ mutant. The axes are colored in red and green for JD and CTD, respectively. Crosslink pairs between JD-CTD, JD-JD and CTD-CTD are shown in a dashed box colored grey, red and green, respectively. Contacts to helix 5 in WT DnaJB8 are denoted with H5. **(i)** Schematic of DnaJB8 species observed in solution based on DLS dimensions. Domains are shown as JD (red spheres), CTD (green spheres), and G/F+S/T (light blue spheres). The average R_h of DnaJB8$_{F\rightarrow S}$ (3.53±0.05nnm) and DnaJB8 *ab initio* Rosetta model (4.02nm) are assigned to the monomer. The R_h of WT DnaJB8 begins as a 4.28nm species and grows to 5.77nm over 20hrs. Size and volume estimates from the structural models suggest DnaJB8 exists as small species ranging from a monomer to octamer likely dominated by a dimer and over time maturing into large oligomers.

Figure 3

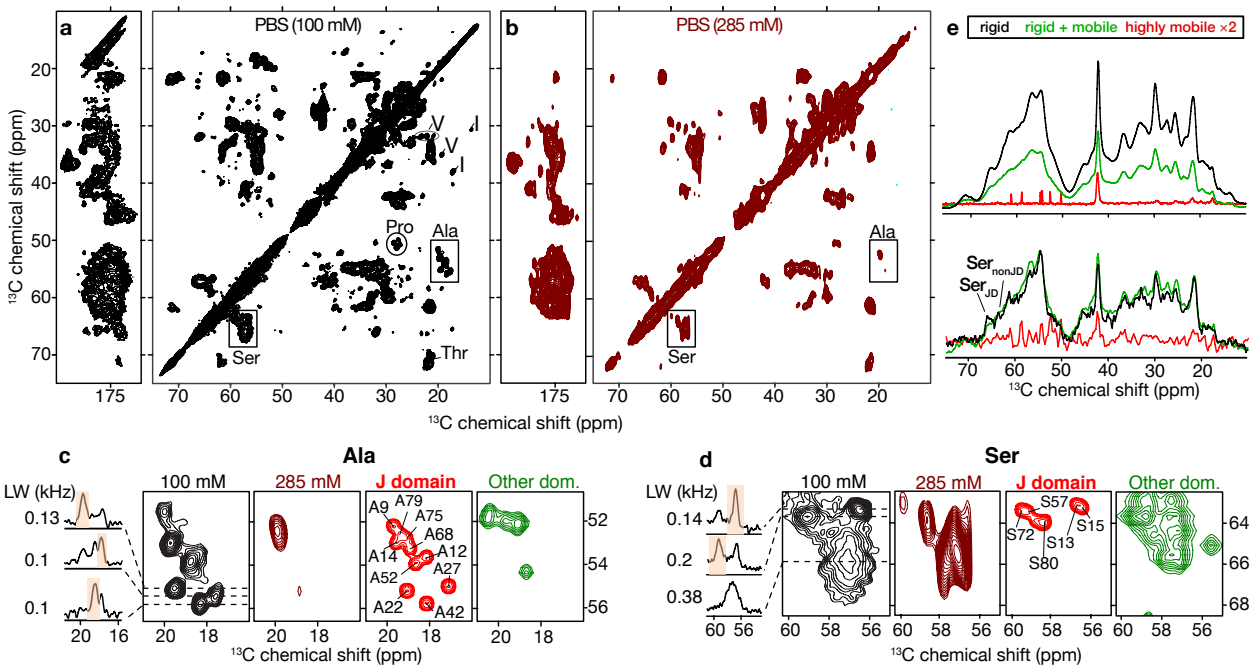

Figure 3. Solid-state NMR of DnaJB8 oligomers at physiological and high ionic strength. (a) 2D ^{13}C-^{13}C ssNMR spectrum of U-^{13}C,^{15}N-labeled DnaJB8 oligomers in PBS (100 mM NaCl), using 25 ms DARR mixing. **(b)** Corresponding 2D ssNMR spectrum in PBS with 285mM NaCl. **(c-d)** Boxed Ala and Ser regions from panels "a" and "b". In PBS, the experimental Ala and Ser peak patterns (black) are well resolved and similar to those expected for folded JD in solution (red). At elevated ionic strength (brown) these narrow peaks are missing. Green spectra (right) represent simulated signals predicted for our models of the non-JD domains, shown with enhanced broadening reflecting the heterogeneity seen in the experiments. 1D spectra on far left show slices through the experimental 2D data, with selected peak widths (in kHz). (**e**) ^{13}C 1D spectra, in PBS (top) and with 285 mM NaCl (bottom), that show rigid residues (black, CP), rigid and mobile residues (green, SPE) and only mobile residues (red, INEPT). See also text and Supplementary Fig. 3.

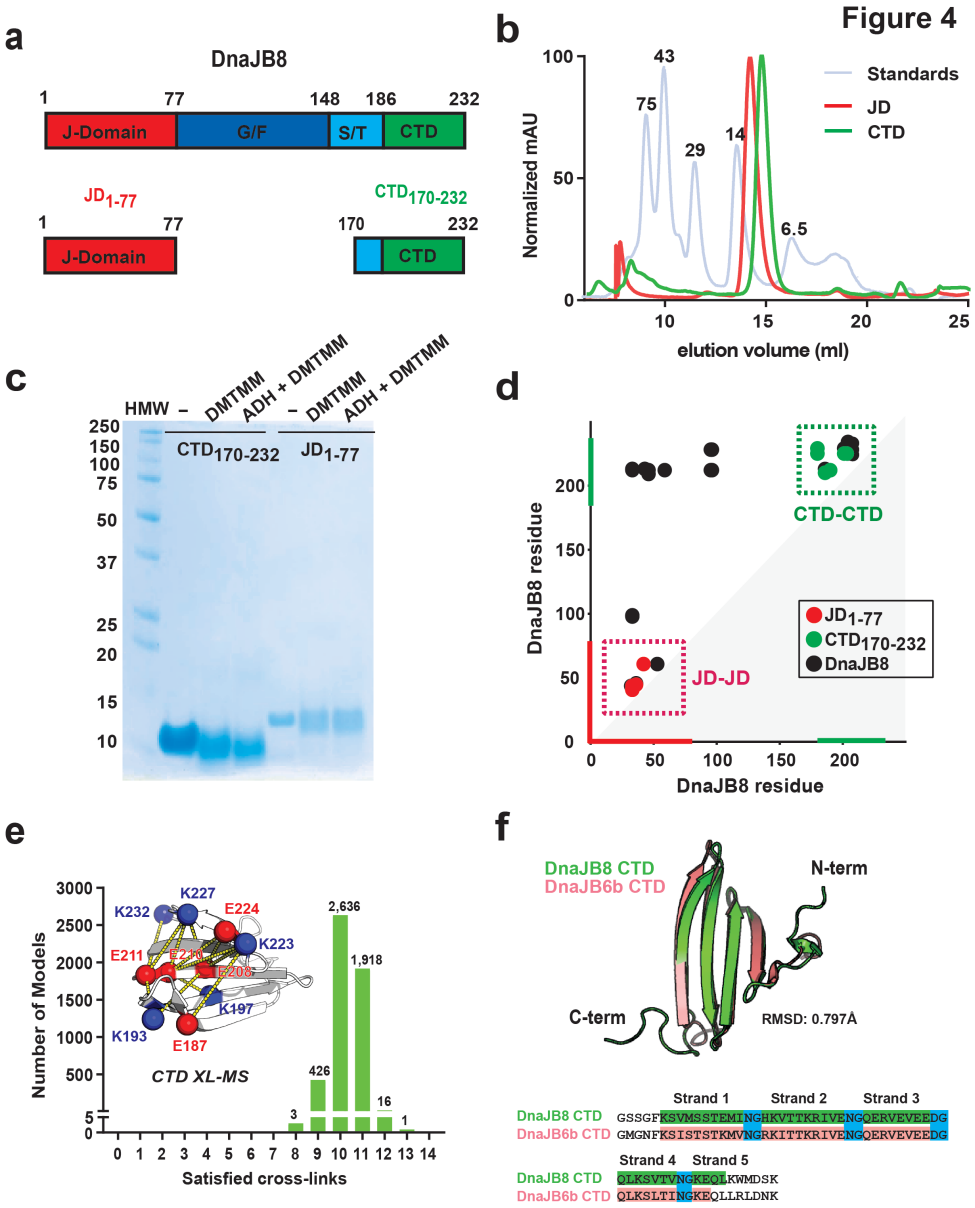

Figure 4. Isolated JD and CTD proteins are monomeric. (a) Cartoon schematic for the full length DnaJB8 and domain fragments JD_{1-77} and $CTD_{170-232}$. **(b)** Representative SEC profiles of JD_{1-77}(red), $CTD_{170-232}$(green) and LMW standards (blue). JD_{1-77} and $CTD_{170-232}$ elute at apparent molecular weights of 14kDa and 6.5kDa, respectively. **(c)** SDS-PAGE coomassie gel of crosslinked JD_{1-77} and $CTD_{170-232}$ reacted with either DMTMM only or DMTMM with ADH. **(d)** Contact map of ADH/DMTMM crosslinks identified for JD_{1-77}(red), $CTD_{170-232}$(green) and full length DnaJB8 (black). The axes are colored in red and green for JD and CTD, respectively. Crosslink pairs between JD-JD and CTD-CTD are shown in dashed boxes colored in red and green, respectively. **(e)** Histogram of the number of intra-domain crosslinks that are consistent with crosslink chemistry geometry ("satisfied") in the ensemble of 5000 models. One model satisfies 13 out of 14 possible crosslinks identified in our experiments. Crosslinks are mapped onto best matching CTD structural model (inset), shown in white cartoon representation. Sites of crosslink are shown as red or blue spheres, for D/E and K, respectively. Dashed yellow lines connect linked

amino acid pairs. **(f)** Overlay of our DnaJB8 CTD model generated by *ab initio* ROSETTA (green) with the published DnaJB6bΔST CTD (salmon) (PDB:6U3R). The CTD sequences of DNAJB8 and DNAJB6 are shown with each β-strand highlighted and conserved NG and DG turns in blue.

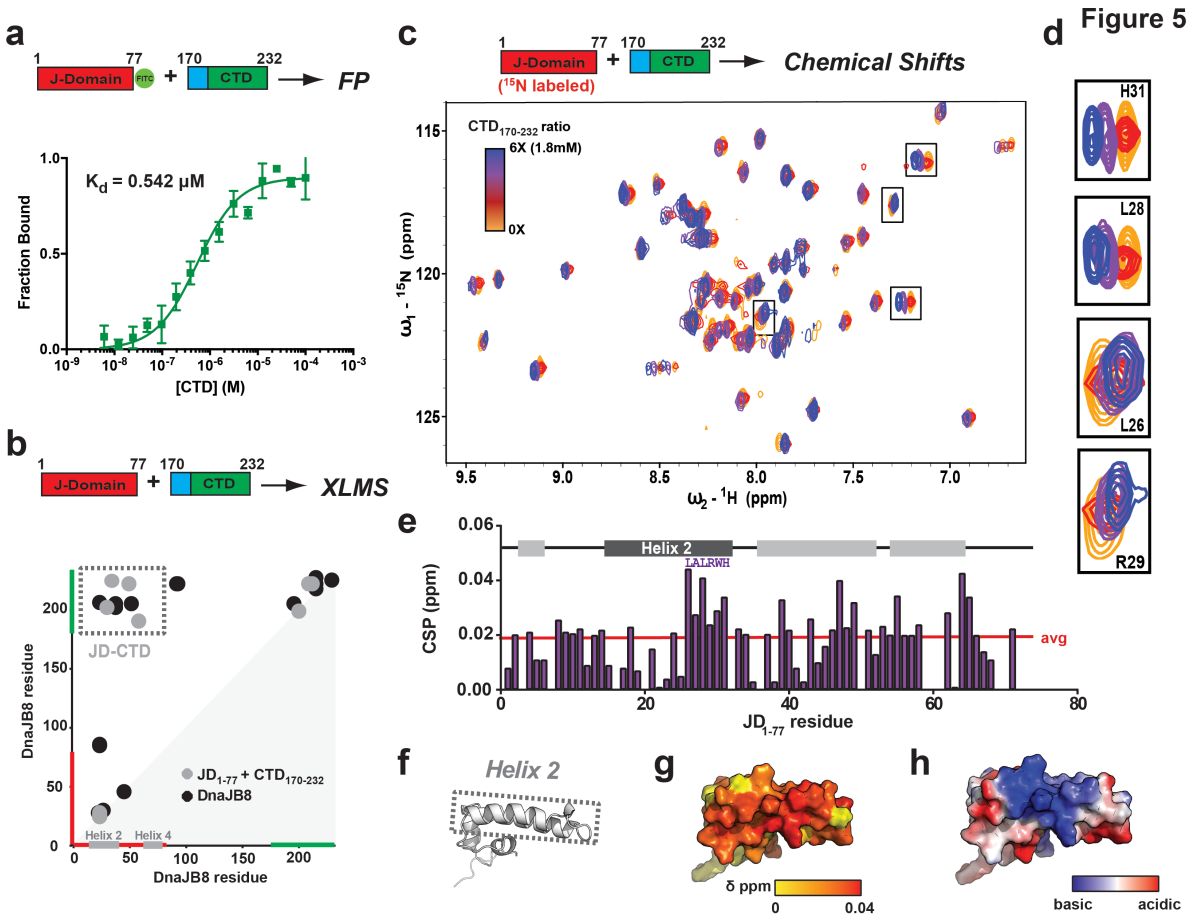

Figure 5. JD and CTD interact through charge complementary surfaces. (a) Schematic of the JD_{1-77}-FITC (FITC dye is shown as a green circle) and $CTD_{170-232}$ constructs used in fluorescence polarization (FP) experiments. FP titration measuring interaction between JD_{1-77}-FITC and a concentration range of unlabeled $CTD_{170-232}$. FP experiments were performed in triplicate and shown as averages with standard deviation. **(b)** Schematic of the JD_{1-77} and $CTD_{170-232}$ constructs used in the XL-MS experiments. Contact map of ADH/DMTMM crosslinks identified from an incubated JD_{1-77} and $CTD_{170-232}$ sample (grey) and full length DnaJB8 (black). The axes are colored in red and green for JD and CTD, respectively. Helix 2 and 3 are shown in grey on the x-axis. Crosslink pairs between JD-CTD are shown in a dashed box colored in grey. **(c)** Schematic for the solution NMR chemical shift experiment with U-^{15}N JD titrated with unlabeled CTD. HSQC solution NMR spectrum of 300μM ^{15}N-labelled JD_{1-77} against a titration of $CTD_{170-232}$: 0x (yellow), 1x (red), 3x (purple), 6x (blue). DnaJB8 JD peak assignments were transferred from deposited data (BMRB:11417). **(d)** Insets of peaks with highest observed chemical shifts: H31, L28, L26, R29. Coloring as in **c**. **(e)** Histogram of chemical shift perturbations (CSP) from 3x CTD experiment by residue. Average CSP of ~0.019ppm is denoted by the red line (excludes prolines). The sequence of last 6 residues of helix 2 are marked above their respective peaks. **(f)** DnaJB8 JD structure illustrating the location of helix 2 (pdbid:2DMX). **(g)** Mapping CSP values onto the DnaJB8 JD structure, shown in surface representation and colored according to $\Delta\delta$ from low (0.0 ppm) in yellow to high (red; 0.04 ppm). **(h)** Electrostatic potential mapped onto DnaJB8 JD structure shown in surface representation. Highly acidic potential is shown in red and highly basic in blue.

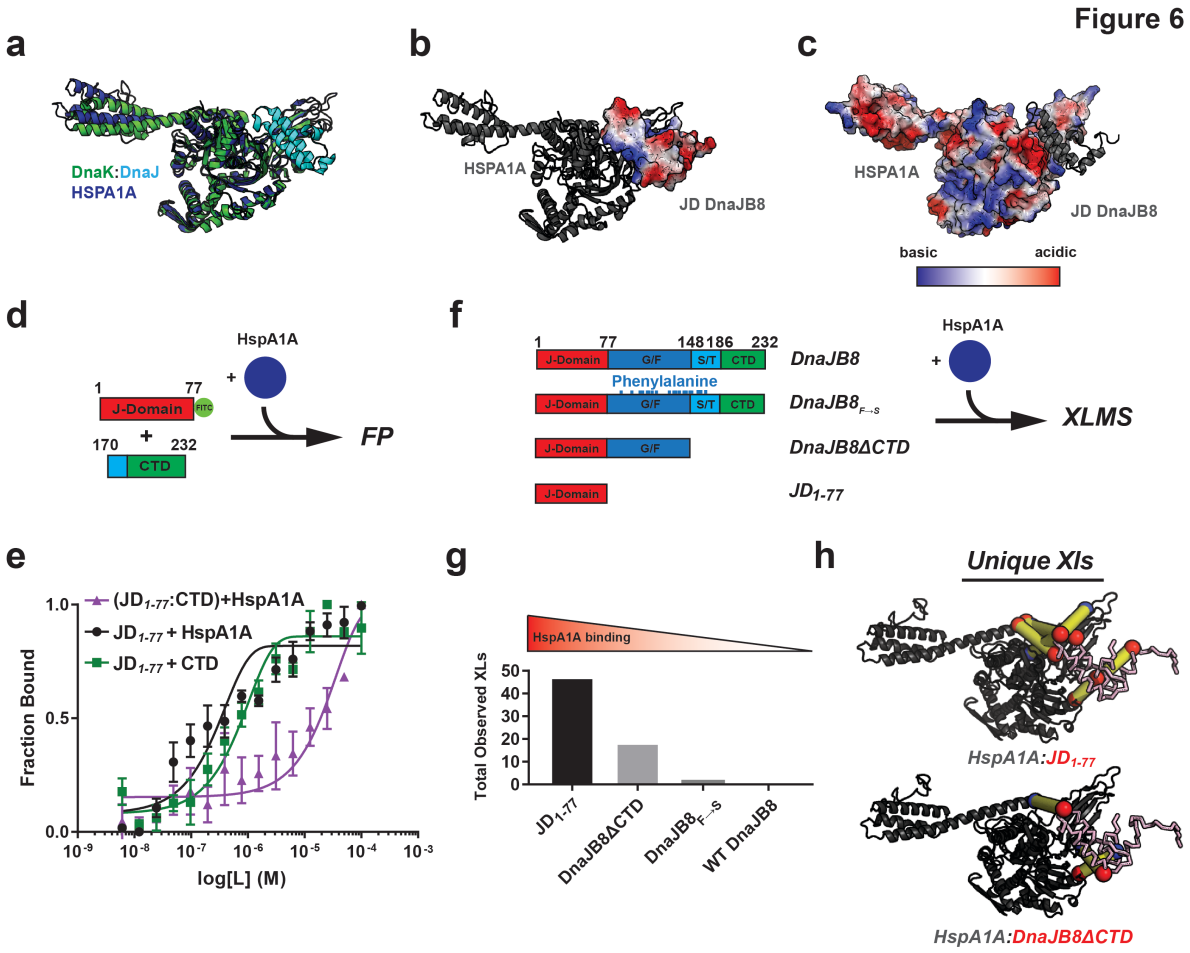

Figure 6. CTD and HSPA1A compete for the same basic binding surface on DnaJB8aD. (a) Structural superposition of a representative HspA1A structural homology model (blue) with a crystal structure of DnaK-DnaJ (green and cyan, respectively; PDBID: 5NRO) shows good agreement. **(b-c)** Electrostatic surface potential of DnaJB8 JD docked into the JD binding site on HspA1A (shown in black cartoon representation). Basic surface on helix 2 docks onto the HspA1A surface. Electrostatic surface potential of HspA1A with docked DnaJB8 JD in black cartoon representation. The HspA1A surface presents an acidic face that complements the basic DnaJB8 JD surface. Highly acidic potential is shown in red and highly basic is shown in blue. **(d)** Experimental workflow used to determine competition between Hsp70 and $CTD_{170-232}$ for JD_{1-77}-FITC binding (dye shown as a green circle). **(e)** Normalized FP binding curves measuring affinity between fluorescent JD and added CTD (green) or added Hsp70 (grey). Preincubation with CTD followed by addition of Hsp70 (purple) shows delay in binding consistent with a competitive binding model. FP experiments were performed in triplicate and shown as averages with standard deviation. **(f)** XL-MS-based experimental workflow used to determine contribution of CTD to regulate JD binding to Hsp70. WT DnaJB8, DnaJB8ΔCTD, $DnaJB8_{F\rightarrow S}$ and JD_{1-77} DnaJB8 variants were used to form complexes with HspA1A. (**g**) Summary of total intermolecular crosslinks identified across three XL-MS experiments between the JD and HspA1A for four complexes: JD_{1-77}:HspA1A, DnaJB8ΔCTD:HspA1A, WT DnaJB8:HspA1A and $DnaJB8_{F\rightarrow S}$:HspA1A. (**h**) Unique intermolecular crosslinks identified across three datasets in the JD_{1-77}:HspA1A and DnaJB8ΔCTD:HspA1A complexes mapped onto the JD-HspA1A model. JD

is shown in pink ribbon representation and HspA1A in black cartoon representation. Sites of crosslink are shown as red or blue spheres for aspartic/glutamic acid and lysine, respectively. Yellow lines connect linked amino acid pairs.

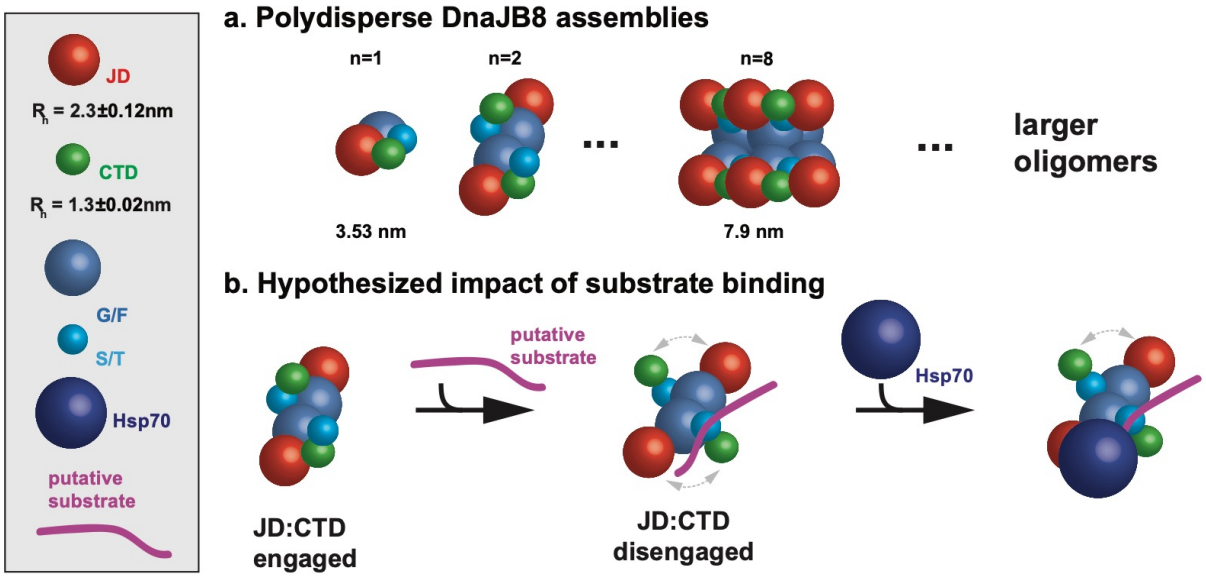

Figure 7. Proposed model for DnaJB8:HspA1A:Substrate relationship
Schematic of proposed DnaJB8 model. Domains are shown as JD (red spheres), CTD (green spheres), G/F (blue spheres), S/T (light blue spheres), and also HspA1A (dark blue spheres) and substrate (purple line) are shown. DnaJB8 domain sizes are displayed scaled to the relative R_h values derived from DLS experiments (HspA1A not drawn to scale). **(a)** DnaJB8 forms a fundamental oligomeric species through aromatic contacts in the G/F and S/T domains ranging from monomer to octamer. **(b)** The JD:CTD engaged state, where the JD is stabilized by CTD and helix 5 (G/F) contacts, can form larger polydisperse oligomers (>100nm). The JD:CTD disengaged state (bottom) is needed to engage with HspA1A. We illustrate our hypothesis where substrate binding may allosterically disrupt the JD:CTD interaction to allow the recruitment of HspA1A to the freed JD-CTD binding face, enabling subsequent handoff of substrate to HspA1A.

1359 **SUPPLEMENTARY INFORMATION**

1360

1361 # Auto-regulatory J-domain interactions control Hsp70 recruitment to
1362 # the DnaJB8 chaperone

1363

1364 Bryan Ryder, Irina Matlahov, Sofia Bali, Jaime Vaquer-Alicea, Patrick C.A. van der Wel, Lukasz
1365 A. Joachimiak

1366
1367
1368
1369
1370
1371
1372
1373
1374
1375
1376
1377
1378
1379
1380

1381 **Supplementary Data**

1382

1383 **Supplementary Data 1. Primary XL-MS data for DnaJB8 and its domains.**

1384 **Supplementary Data 2. Primary DLS measurements for DnaJB8 oligomers.**

1385

1386

1387

1388

1389

1390

1391

1392

1393

1394

1395

Supplemental Tables

Supplementary Table 1. Residue distribution per domain with net charge for each domain.

Domain aa. length	Domain	Residue																				Net charge for the domain
		A	R	N	D	Q	E	G	H	I	L	K	M	F	P	S	T	Y	V	W	C	
1-75	**JD**	8	5	3	6	1	7	2	1	1	6	10	1	1	3	7	0	5	4	2	1	+2
76-148	**G/F**	6	5	2	5	0	5	13	2	1	2	0	1	14	6	6	3	2	0	1	0	-5
149-185	**S/T**	0	0	1	0	0	1	7	1	0	1	1	3	4	0	15	4	0	1	0	1	0
186-232	**CTD**	0	2	3	2	3	6	4	7	2	2	6	1	0	0	2	3	0	6	1	0	0

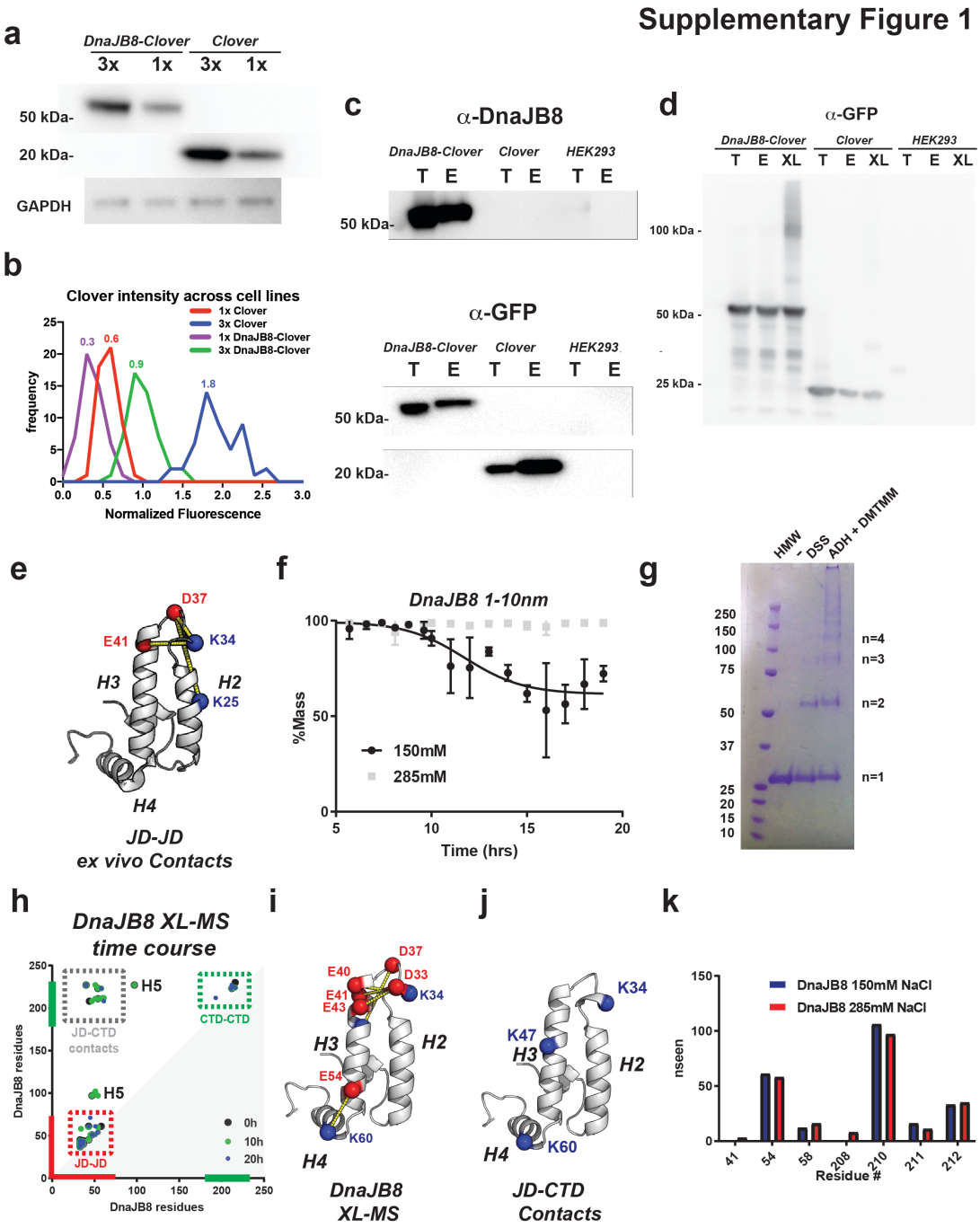

Supplementary Figure 1. Biochemical and mass spectrometry analysis of DnaJB8 in cells and *in vitro*. (a) Western blot analysis of 1x DnaJB8-Clover, 3x DnaJB8-Clover, 1x Clover and 3x Clover cell lines to quantify levels of expression in each cell line. GAPDH western blot is shown as a loading control. (**b**) Normalized FITC intensity analysis of 1x Clover (red), 3x Clover (blue), 1x DnaJB8-Clover (purple) and 3x DnaJB8-Clover (green) cell lines. Intensity measurements were calculated from 50 images for each cell line and the signal normalized to DAPI fluorescence intensity. (**c**) Western blot analysis of input and anti-GFP nanobody elutions DnaJB8-Clover, Clover and HEK293 cell lines as detected with anti-DnaJB8 and anti-GFP antibodies. Total (T) and elutions (E) for each condition are shown. (**d**) Western blot analysis of DnaJB8-Clover and

1437 Clover proteins isolated from mammalian cell lines. Total (T), elutions (E) and crosslinked elutions
1438 (XL) of each condition are shown. Western blot was probed with GFP antibodies. **(e)** JD intra-
1439 domain ADH/DMTMM crosslinks identified from DnaJB8-Clover isolated from cells mapped onto
1440 the JD structure. JD is shown in cartoon representation and is colored in white. Sites of crosslink
1441 are shown as spheres and are colored red or blue for aspartic/glutamic and lysines, respectively.
1442 Dashed yellow lines connect linked amino acid pairs. **(f)** DnaJB8 particles with a R_h of 1-10nm in
1443 the DLS data were analyzed by proportion of the total sample (% mass) and binned by the size
1444 distribution of the constituent particles. The time evolution of this mass fraction is shown for
1445 150mM NaCl (black) and 285mM NaCl buffer conditions in 1xPBS. **(g)** SDS-PAGE coomassie
1446 gel showing DnaJB8 in the absence of crosslinker (left), with DSS (middle), and with DMTMM
1447 and ADH (right). **(h)** XL-MS contact map of DnaJB8 crosslinks identified using DMTMM and ADH
1448 from a time course: t=0hrs (large black dot), t=10hrs (medium green dot) and t=20hrs (small blue
1449 dot), small. The axes are colored in red and green for JD and CTD, respectively. Crosslink pairs
1450 between JD-CTD are shown in dashed box colored grey, red and green, respectively. Helix 5
1451 crosslinks are denoted by H5. **(i)** JD intra-domain ADH/DMTMM *in vitro* crosslinks mapped onto
1452 the JD structure. JD is shown in cartoon representation and is colored in white. Sites of crosslink
1453 are shown as spheres and are colored red or blue for aspartic/glutamic and lysines, respectively.
1454 Dashed yellow lines connect linked amino acid pairs. **(j)** Three *in* vitro JD-CTD inter-domain
1455 ADH/DMTMM crosslinks mapped onto the JD structure. DnaJB8 JD is shown in cartoon
1456 representation and is colored in white. JD lysine sites that crosslink to CTD are shown as spheres
1457 and are colored blue. **(k)** Histogram of frequency of ADH monolinks observed in normal and
1458 elevated ionic strength XLMS experiments.
1459
1460
1461
1462
1463
1464
1465
1466
1467
1468

Supplementary Figure 2

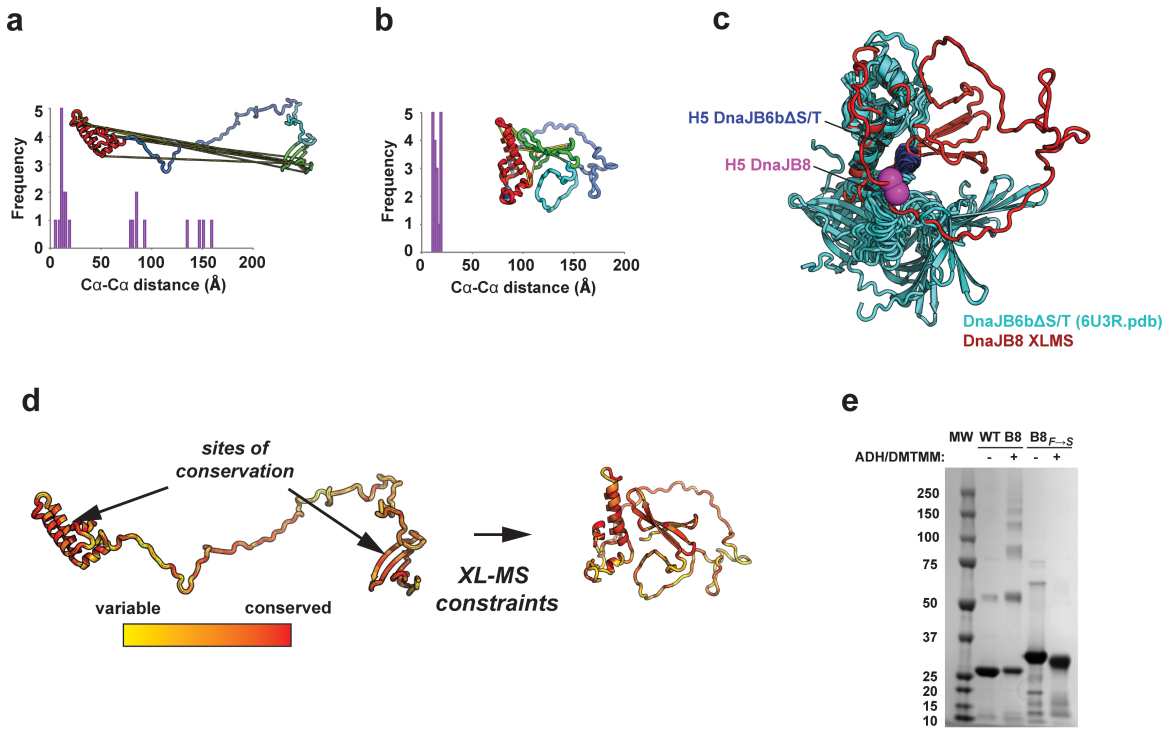

Supplementary Figure 2. Modeling the full length DnaJB8 monomer using crosslinks. (a) DnaJB8 ADH/DMTMM crosslinks mapped onto an expanded structure featuring the conserved JD and our predicted CTD model. The histogram of C_α-C_α distances shows 11 crosslinks that exceed the physical limitations for ADH/DMTMM. **(b)** Rosetta *ab initio* collapsed structure of DnaJB8 with ADH/DMTMM crosslinks mapped. The histogram of C_α-C_α distances shows that all crosslinks are satisfied when the JD and CTD are docked in this model. **(c)** Overlay of our Rosetta *ab initio* collapsed structure (red) with the solution NMR ensemble of the published DnaJB6bΔST deletion variant (cyan; PDBID: 6U3R) The proposed helix 5 (H5) is shown on the DnaJB8 (pink) and DnaJB6bΔST (blue) models. The position of H5 in our DnaJB8 XL-MS-constrained model is close to the position in the DnaJB6b model. The major difference is the position of the CTD, which is influenced by both the XL-MS constraints, and the inclusion of the S/T region that was deleted in the DnaJB6b construct. **(d)** Conserved surfaces on the JD and CTD in the full-length DnaJB8 model mediate the interaction. Highly conserved sites are colored in red (and highlighted by arrows) and variable positions are colored in yellow**.** Sequence-based conservation of DnaJB8 shows highly conserved faces along the JD, and some conserved faces in the CTD that overlap with the XL-MS identified surfaces. **(e)** SDS-PAGE coomassie gel of DnaJB8 and DnaJB8$_{F\rightarrow S}$ mutant crosslinked with ADH/DMTMM.

Supplementary Figure 3

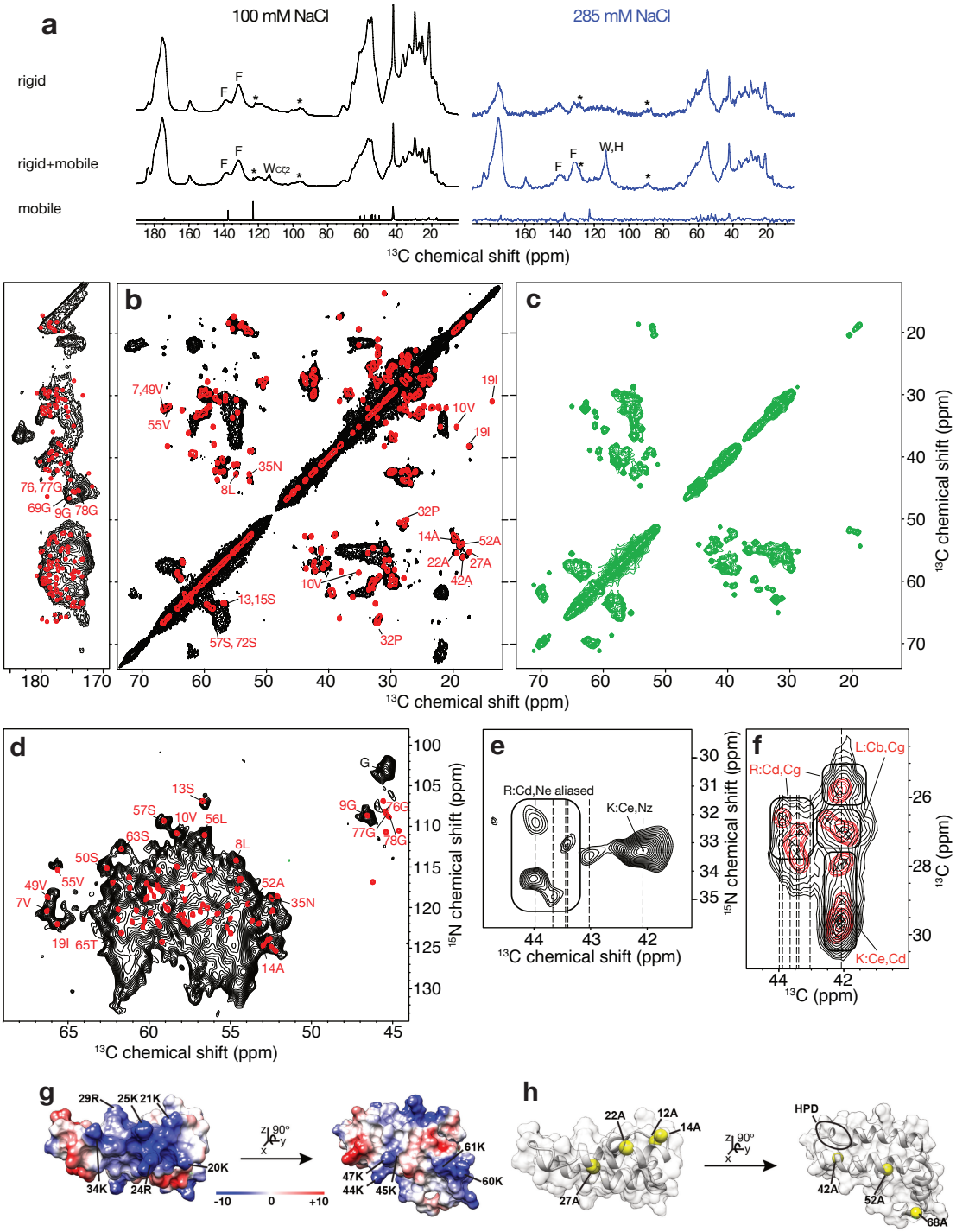

Supplementary Figure 3. Additional ssNMR data and analysis for DnaJB8 oligomers in PBS. (a) ^{13}C 1D spectra at 100mM NaCl (black) and elevated ionic strength (blue) that show rigid residues (CP), rigid and mobile residues (SPE) and only mobile residues (INEPT). **(b)** Overlay of the experimental (black) 2D ^{13}C-^{13}C CP-DARR spectrum of DnaJB8 oligomers uniformly labeled

with ^{13}C and ^{15}N and synthetic (red) spectrum of the DnaJB8 JD in solution generated from BMRB chemical shifts (red assignments). **(c)** Simulated spectrum from three other domains (G/F, S/T and CTD), showing diagonal peaks and one-bond cross-peaks involving backbone $C\alpha$-$C\beta$ and CO-$C\alpha$ carbons. **(d)** 2D ^{13}C-^{15}N CP-based NCA experimental spectrum (black) of DnaJB8 oligomers uniformly labeled with ^{13}C and ^{15}N, overlaid with synthetic spectrum of the DnaJB8 JD in solution (red) from BMRB chemical shifts (red assignments). **(e)** 2D CP-based ^{13}C-^{15}N spectrum with $C\varepsilon$-$N\zeta$ and (aliased) $C\delta$-$N\varepsilon$ correlations from immobilized Lysine and Arginine side chains, respectively. **(f)** Enlarged ^{13}C- C spectral region from panel (A) demonstrating good alignment of Arg, Lys and Leu signals between experimental ssNMR (black) and solution chemical shifts of the JD (red). Dashed lines mark known ^{13}C positions used to confirm amino acid types of signals. **(g)** Electrostatic surface potential of the DnaJB8 JD, with selected residues indicated. Highly positive and negative potentials are colored blue and red, respectively. White color represents neutral charge. **(h)** The same view showing the location of Ala with narrow peaks at 100 mM NaCl which disappear at 285 mM NaCl (Fig. 3, panel “c”).

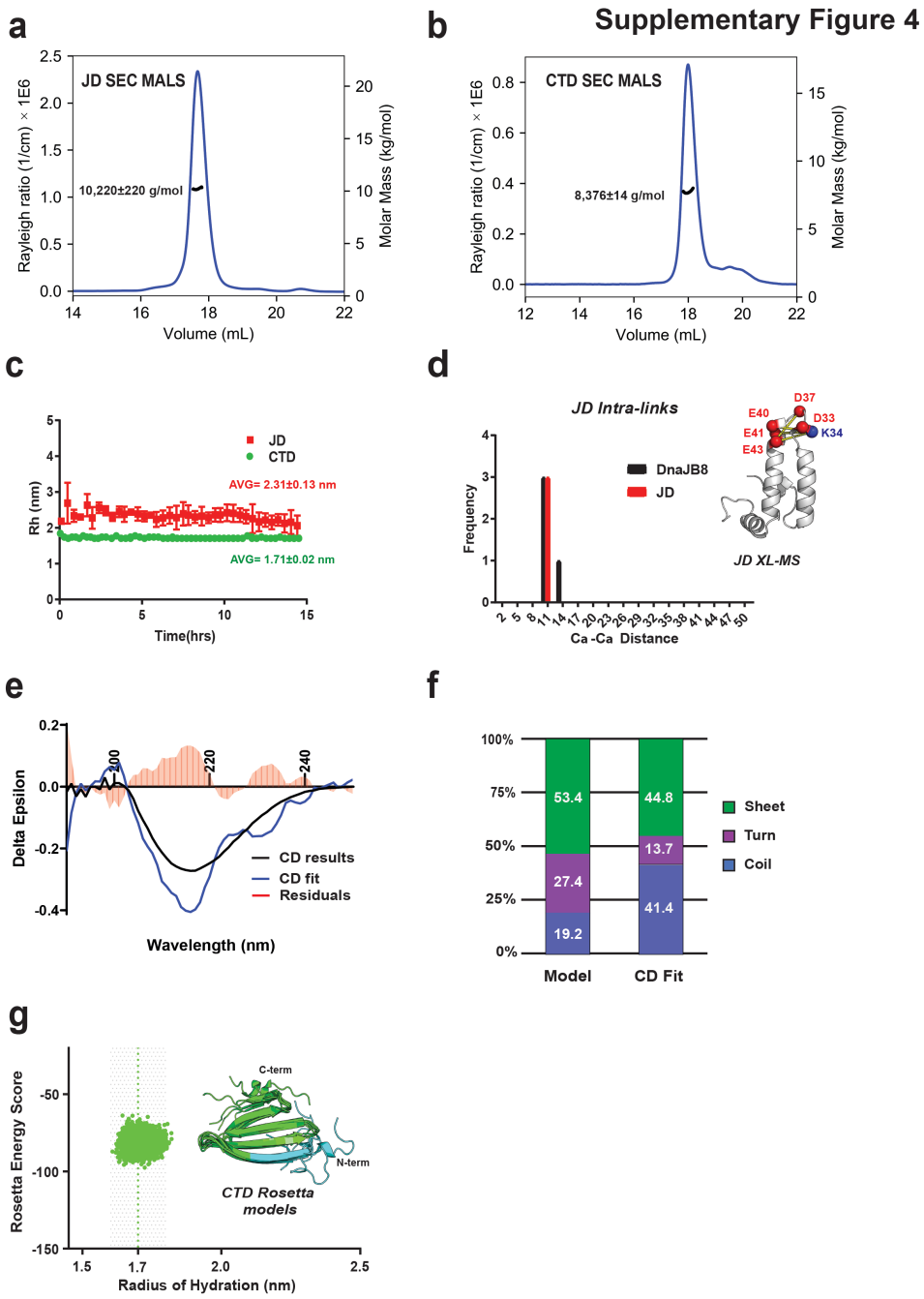

Supplementary Figure 4. JD and CTD are stable monomers. (a) SEC-MALS of JD_{1-77} shows a single peak with a calculated molar mass of 10,220 ± 220 g/mol consistent with a monomer. **(b)** SEC-MALS of $CTD_{170-232}$ shows a single peak with a calculated molar mass of 8,376 ±14 g/mol consistent with a monomer. **(c)** DLS time course of JD_{1-77} and $CTD_{170-232}$ constructs. The average R_h of JD_{1-77} and $CTD_{170-232}$ was calculated to be 2.30±0.12 nm and 1.71±0.02 nm, respectively. **(d)** Histogram of JD intra-domain crosslinks across XLMS experiments for DnaJB8(black), JD_{1-77}(red), and JD_{1-77} mixed with $CTD_{170-232}$(grey). All intra-domain crosslinks satisfy the physical constraint of <20nm for the ADH/DMTMM crosslinkers. **(e,f)** CD spectra of CTD was analyzed using the Bestsel server. Secondary structure analysis of the data shows high β-sheet character

(yellow) with some helix character (purple) and no random coil (blue). The results are compared to the CTD model generated from ab initio. **(g)** 5,000 Rosetta *ab initio* generated models of CTD. The structural models are consistent with R_h values derived from DLS (dashed line). Structural overlay of low energy scoring models reveals consistent pleated beta-sheet fold. Models are shown in cartoon representation and are colored in green.

Supplementary Figure 5

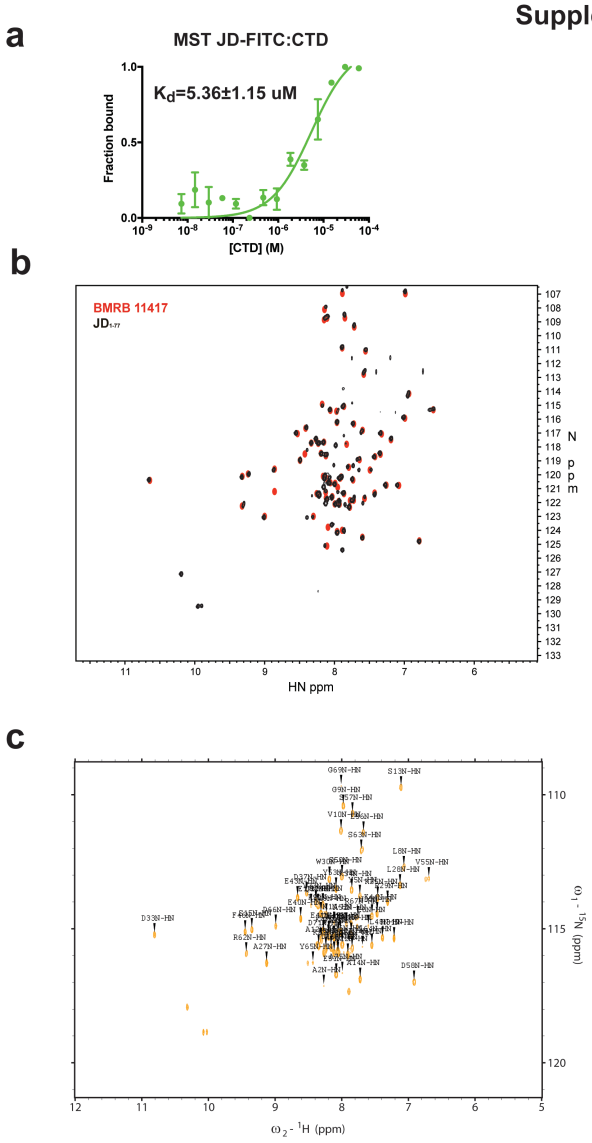

Supplementary Figure 5. $JD_{1\text{-}77}$ construct spectra consistent with deposited chemical shifts. (a) Microscale Thermophoresis measurements of $JD_{1\text{-}77}$-FITC binding to $CTD_{170\text{-}232}$. Measurements were performed in triplicate using 200nm $JD_{1\text{-}77}$-FITC and a range of $CTD_{170\text{-}232}$. The samples were incubated and measured in a Monolith NT.115 instrument. The data were processed using PALMIST software and the normalized fluorescence values plotted as an average across three replicates with standard deviations **(b)** Overlay of our ^{15}N-^{1}H HSQC spectra for $JD_{1\text{-}77}$(black) onto the submitted spectra for DnaJB8 JD (red) (BMRB:11417). 97% of assigned peaks in the published spectra were matched to our data. (**c)** Amino acid assignments mapped onto the HSQC spectra for the $JD_{1\text{-}77}$ protein.

Supplementary Figure 6

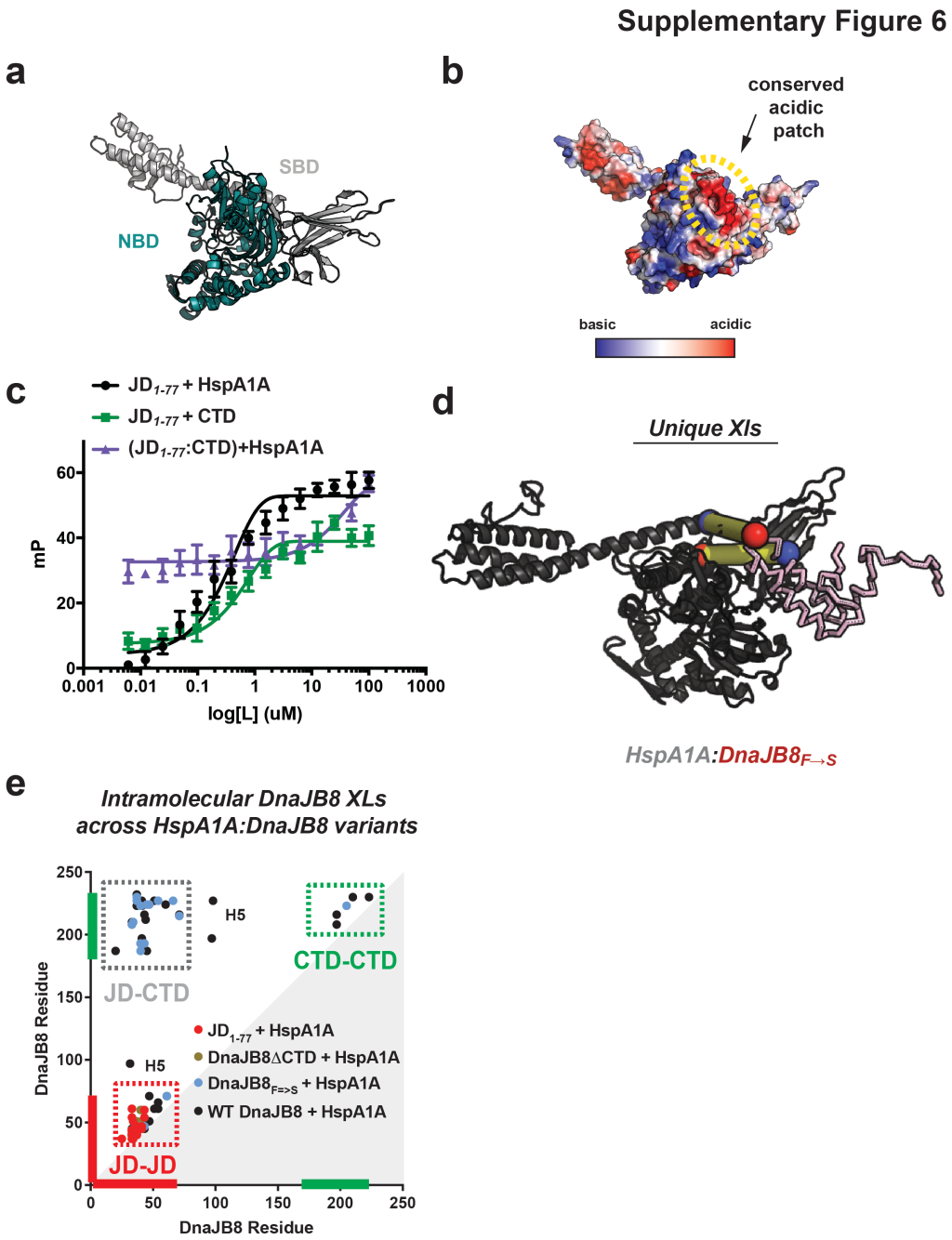

Supplementary Figure 6. Hsp70 proteins present a conserved acidic surface. (a) Structure of HspA1A colored by domain with the nucleotide binding domain (NBD) in turquoise and substrate binding domain (SBD) in grey. (**b)** Electrostatic surface mapped onto the HspA1A structure with the negatively charged Hsp40-JD-binding site circled in yellow. **(c)** Raw FP binding curves of labeled JD mixed with HspA1A (black), with CTD (green) and (JD-CTD)+HspA1A (purple). Y-axis is defined as milipolarization (mP). FP experiments were performed in triplicate and shown as averages with standard deviation. **(d)** The two intermolecular crosslinks identified across three XL-MS datasets between JD and HspA1A in the DnaJB8:HspA1A complex mapped onto JD-HspA1A model. JD is shown in ribbon representation and HspA1A in cartoon representation, colored pink and black respectively. Sites of crosslink are shown as red or blue

1584 spheres for aspartic/glutamic acid and lysines, respectively. Yellow lines connect linked amino
1585 acid pairs. **(e)** XL-MS contact map of changes in intramolecular DnaJB8 crosslinks identified
1586 using DMTMM and ADH in co-mixtures of different variants of DnaJB8 with HspA1A: WT
1587 DnaJB8:HspA1A (black), DnaJB8ΔCTD:HspA1A (brown), $DnaJB8_{F\rightarrow S}$:HspA1A (blue) and JD_{1-77}:HspA1A (red). The axes are colored in red and green for JD and CTD, respectively. Crosslink
1589 pairs between JD-CTD are shown in dashed box colored grey, red and green, respectively.
1590 Contacts to helix 5 in WT DnaJB8 are denoted with H5.